Dissertations, Theses, and Masters Projects   Theses, Dissertations, & Master Projects

1990

A Numerical Model Study of Estuarine Residual Circulation and Stratification Variations during Spring-Neap Tidal Cycles

San Jin
College of William and Mary - Virginia Institute of Marine Science

Follow this and additional works at: https://scholarworks.wm.edu/etd

Part of the Oceanography Commons

A Numerical Model Study of Estuarine Residual Circulation

and Stratification Variations During Spring-Neap Tidal Cycles

————

A Thesis

Presented to

The Faculty of the School of Marine Science

The College of William and Mary

In Partial Fulfillment

Of the Requirements for the Degree of
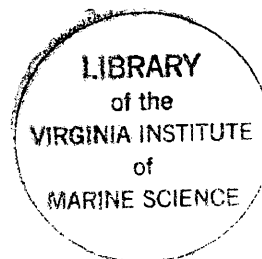
Master of Arts

————

by

San Jin

1990

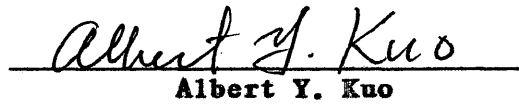# APPROVAL SHEET

This thesis is summitted in partial fulfilment of

the requirements for the degree of

Master of Arts

_____
San Jin

Approved, May 1990

_____
John H Hamrick, Chairman

_____
Albert Y. Kuo

_____
Bruce Neilson

_____
Evon Ruzecki

_____
Eugene H Burreson

TABLE OF CONTENTS

ACKNOWLEDGEMENTS

LIST OF FIGURES

ABSTRACT

An accurate two dimensional (vertical plane) finite difference model was developed to simulate a real-time flow in a partially mixed estuary with a spring-neap tide forcing. The numerical model is based on primitive equations, and is a time-dependent, stretched-z coordinate model with an algebraic stress/flux turbulence model incorporated into it. An implicit numerical scheme in the vertical direction and a mode-splitting technique are used to improve computational efficiency which makes long-term real time simulations and numerical experiments possible.

The instantaneous output from the model is processed by a harmonic least squares filter to extract the modulated residual currents, such as Lagrangian residual, Eulerian residual, Stokes drift and vector potential transport residual. These residual currents are analyzed for their roles in the stratification-destratification processes in the simulated estuary of 150 km with a depth of 10 meters.

The numerical experiments show that near the channel mouth where water columns are well mixed vertically during the spring-neap cycle, vector potential transport velocity, which is a part of the Stokes drift in stretched coordinate, is mainly responsible for the weakening of the Lagrangian residual velocity during the spring tide both in the surface and the bottom layers, while in the channel middle, the turbulent mixing is mainly responsible for the destratification of the channel during the spring tide period, the nonlinearly induced currents play only a secondary role.

A Numerical Model Study of Estuarine Residual Circulation

and Stratification Variations During Spring-Neap Tidal Cycles

1. Introduction

1.1   Background Discussion

Estuaries are regions of water, which are connected to the sea
or ocean at one end and fed by sources of fresh water (rivers) at the
landward boundaries. In these regions saline sea-water and fresh river
water meet and mix in an unsteady environment which is influenced by
tides, winds, variable density, the earth's rotation, and the shape of
the coastal system. Simulation and prediction of the resulting flow
field and salinity field distribution is a complex hydrodynamic
problem.

Early investigations of the circulation within an estuary were
approached either through complicated analytical studies under some
simplifying assumptions, such as a rectangular channel and the neglect
of non-linear terms (Hansen and Rattray, 1965), or by reduced scale
hydraulic model or field measurements (Hudson 1979, Pritchard 1954,
1956). It is usually quite difficult to get an over-view of the
instantaneous circulation pattern and density field from field
measurements because of the prohibitive cost involved in obtaining
adequate spatial and temporal average.

With significant advances in both the availability of digital
computers with a very high computation speed and the improved
understanding of the numerical methods for solving partial

2

differential equations, numerical simulation is quickly becoming a very powerful and practical tool for solving hydrodynamic problems. Research work in climatic modeling has shown that this approach is both economical and flexible and can succeed where multiple physical processes simultaneously influence the flow dynamics. Numerical simulation is generally based on the time integration of the primitive equations of motion starting from a fictitious initial field. Because of the ease with which various physical processes can be incorporated, numerical simulation of estuarine process can not only be useful in making management decisions, but can also play a very important role in probing theoretical ideas which are put forward to explain various phenomena in estuaries.

Partially stratified estuaries are very common in the east coast of North America. They have a characteristic two-layer circulation when averaged over several tidal periods, with fresher surface water showing a net outflow and bottom saltier water a net inflow. Owing to the classical work of Prichard (1956) and others (Bowden, 1967, Hansen 1967), the primary driving force for circulation was shown to be the longitudinal depth varying pressure gradient, balanced by the vertical gradient of the turbulent shear stress. According to this theory, the nonlinear terms in the equations of motion are explicitly ignored as being of secondary importance. However, it can be shown by **perturbation analysis** (Ianniello, 1977) that the magnitude of the non-linearly induced residual current might be of the same order as the gravitational circulation currents in a partially stratified estuary with relatively strong tidal currents and

3

weak density gradients. Since the long-term distribution of the dissolved and suspended biogeochemical constituents depends on the residual currents, not tidal currents, the understanding of nonlinearly induced residual currents is indispensible for long-term prediction of the ecological, geological, chemical, and biological processes in estuaries.

The destratification and stratification associated with the spring-neap tidal cycle in the mid-channel of a partially mixed estuary is very important for the production of phytoplankton because it transports nutrients to the surface water from the bottom water. This phenomena has been explained mainly through the turbulent mixing of fresh surface water with the salty bottom water (Ruzecki, 1986). The vertical gradients of salinity change with the changing mixing energy due to slow modulation of astronomical tidal forcing. Spring tides produce strong currents, and hence strong mixing and destratification, while neap tides produce weak currents, and hence weak mixing and allow the gravitational circulation to re-establish stratification.

Early research work on the application of numerical models to estuaries include Oey et al.'s work on the Hudson-Raritan estuary (1985) which dealt with the mechanisms of the real time salt mixing in the estuary, Cheng's work (1983) in which an attempt was made to define the relation between the Lagrangian residual current and the tidal current phase, and Feng et al.'s (1986) work in South San Francisco Bay (2-D horizontal) which investigated the long-term transport of tracers by the residual currents in the Bay. In

literature, there have been no attempt at exploring the role of the residual currents in the estuary stratification-destratification processes using a numerical model. An attempt is made, in this research work, to build an accurate two dimensional vertical plane numerical model with an algebraic stress/flux turbulence model incorporated into it to simulate the real time flow in an estuary, and to use this numerical model to explore the importance of the second order nonlinearly induced residual currents in the spring-neap cycle of stratification.

In considering steady second order residual currents, a distinction must be made first between the **Lagrangian residual current**, which is defined as **the mean velocity of a marked water parcel**, and the **Eulerian residual current**, which is defined as **the mean velocity at a particular point** in the current field. As is shown by the analysis of Longuet-Higgins (1969), the two velocities could be quite different in some cases. The **difference** is the **Stokes drift, which is caused by a given water parcel** being carried through a spatially varying velocity field during one cycle of an oscillating flow with its trajectory not closed resulting in a net drift. The analytical results for the Eulerian and Lagrangian residual currents induced by the nonlinear interactions of the first order tides exist for a typical **homogeneous** narrow tidal channel of constant breadth, depth and rectangular cross-section under the conditions of zero fresh water discharge and some pre-prescribed eddy viscosity profiles(Ianniello, 1977). With those conditions, the Eulerian residual currents are predominantly seaward at all depths and

therefore will reinforce any two-layer gravitational circulation in the surface waters, but oppose them in the bottom waters, whereas the Lagrangian residual currents oppose the two-layer gravitational circulation in both the surface and bottom waters.

1.2   Objectives and Hypothesis

To gain an insight into spring-neap tidal mixing, an accurate intratidal 2-D (vertical plane) numerical model with an algebraic stress/flux turbulence model incorporated into it is developed to simulate the real-time flow in a partially mixed estuary under spring-neap tide forcing. A least squares harmonic analysis method is used to filter the spring-neap modulated residual currents from tidal currents. The two major objectives of this study are to develop a two dimensional vertical plane numerical model, with a turbulence model which account for the effects of stratification, and to use the model to investigate the role of the modulated residual circulation and vertical mixing in spring-neap tide variations of salinity stratification. The hypothesis to be tested as part of the second objective is that spring neap modulation of the Stokes drift contribution to the Lagrangian residual circulation in an estuary is sufficiently large to result in variations in estuarine stratification. The response of the modulated residual currents, such as Lagrangian residual, Eulerian residual and vector potential transport velocity, to the spring-neap tidal forcing will be examined. Special attention will be directed to the relationship between residual currents and stratification-destratification of the estuary.

7

2. Formulation of the Model Equations

2.1   Three-Dimensional Hydrodynamic Equations

The general cartesian coordinate system for a three dimensional estuary model is shown in Figure 2.1.

where $x_1 = x$ and $x_2 = y$ are horizontal, z is vertical, h is the still water depth, and η is the surface elevation.

Figure 2.1   The Cartesian Coordinate System for a Three

Dimensional Estuary Model
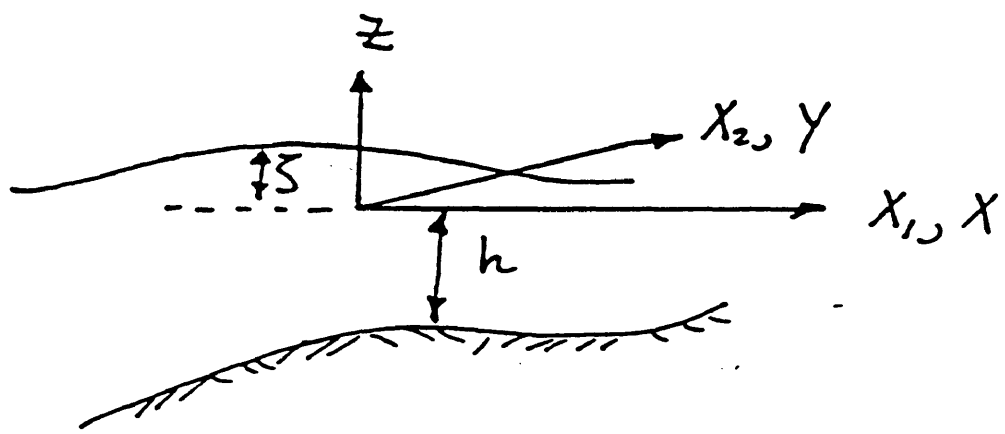
The fundamental physical principles governing motion of water masses in an estuary are the laws of conservation of momentum, mass and energy. Their mathematical expressions are the equations of motion, the continuity equation and the thermodynamic energy equation. In this work, the thermodynamic energy equation is not necessary since temperature changes will not be considered. The starting point for estuary modeling is the Navier-Stokes equations and it's corresponding mass transport equation which describe fully the motion of water and the transport of mass in an estuary including detailed turbulence structure. In principle, circulation in an estuary can be found by solving these differential equations numerically. However, it is not practical to solve these equations in their full generality not only because current computer capacity is still far from being able to solve full Navier-Stokes equation but also because such a brute-force procedure would not provide any insight into the dynamics of the system. It would be quite difficult to understand and interpret the effects of various factors affecting the dynamics of the system from the instantaneous output with fluctuating and average components mixed together.

Generally, two useful approximations are introduced into the Navier-Stokes equations to derive equations for estuary circulation modeling. The first one is that an estuary with depth much less than its horizontal dimensions can always be treated as if the vertical force balance is approximately in hydrostatic equilibrium. This assumption eliminates vertical accelerations due to buoyancy effects and therefore precludes the explicit treatment of free convection

associated with unstable stratification. The second approximation

assumes that density variations may be neglected in the equations of

motion except in the buoyancy term. The latter approximation is known

as the Boussinesq approximation. In addition to the above two

assumptions, from an engineering point of view, there is really no

need to know all the details of the motion of water in an estuary, the

time-average quantities over a short time period compared to tidal

cycle (but long enough to smooth out turbulent fluctuations) are quite

adequate for practical purposes. Instead of explicitly treating the

whole spectrum of motions in an estuary which may range from the

dimensions of the estuary itself to small scales where turbulence

dissipates into heat, the dynamical equations must first be

reformulated to take into account only part of the spectrum. The

implicit assumption here is that it is possible to simulate large

scale organized water motions without a detailed treatment of the

smaller scale turbulent motions. It is hoped that the interactions and

exchange of energy between these two components of flow can then be

approximated by an appropriate parameterization in terms of the large

scale flow. For this purpose, the traditional Reynolds average

procedure is often invoked, which consists of decomposing all

variables into mean and fluctuating components, where the mean value

should be visualized as the result of a low-pass filtering procedure.

After the decomposed variables have been substituted into the Navier-

Stokes equation, the latter equations are averaged by the same rule by

which the mean components have been defined. In this process,

nonlinear terms in the equations generate the correlations between the

fluctuating components which are usually referred to as the Reynolds stress or the Reynolds fluxes. After the Reynolds average procedure, the Reynolds averaged three-dimensional equation of motion and the continuity equation under the assumption of hydrostatic and Boussinesq approximations result. To facilitate finite difference numerical procedures, it is advantageous to further introduce stretched vertical coordinate which transforms both the surface and bottom on to coordinate surfaces. Numerical solution can then be carried out in a rectangular region regardless of the bottom topography. Figure-2.2 shows the transformation from the cartesian to the stretched vertical coordinates for estuary modeling. It is noted that z^{*} is the vertical coordinate in the stretched coordinate.

Figure 2.2   Transformation from the Cartesian to Stretched

Vertical Coordinate
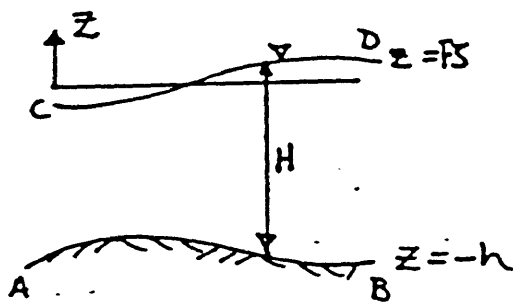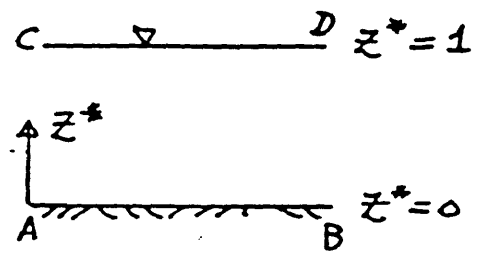
Physical   Computational (Stretched)

It is also advantageous to do scaling analysis for those equations so that the relative importance of each term in the equations can be shown. After the introduction of the stretched coordinate and the scaling analysis procedure, the dimensionless equations in a stretched vertical coordinate system (Hamrick, 1990) are (note: the * is omitted now for all z^*):

Momentum equations:

$$\partial_t(Hu_\alpha) - e_{\alpha\beta}(f)F_R u_\beta H + F\partial_{x\beta}(Hu_\alpha u_\beta) + F\partial_z(wu_\alpha) \qquad (2.1.1)$$

$$= -H\partial_{x\alpha}p_s - (g)H\partial_{x\alpha}\eta - (g')\frac{F}{F_D^2}H\partial_{x\alpha}(H\int_z^1 sdz)$$

$$+ (g')\frac{F}{F_D^2}Hs\partial_{x\alpha}((1-z)h - zF\eta) + \partial_z\tau_{\alpha z} + \delta\partial_{x\beta}(H\tau_{\alpha\beta})$$

where α = 1 or 2, β = 1 or 2 (note x_1 = x, x_2 = y) and Einstein summation rule is assumed in the above equations, and

$$e_{\alpha\beta} = \begin{vmatrix} 0 & 1 \\ -1 & 0 \end{vmatrix}$$

In equation (2.1.1), u_α is the horizontal velocity (α = 1, 2, u_1 is the x component of velocity and u_2 the y component of velocity), w the vertical velocity in the stretched vertical coordinate, $0 < z < 1$ (dimensionless), p_s is the surface pressure, which in our case can be set to a constant of one atmospheric pressure, η the free surface

14

displacement, $H=h+F\eta$, the total depth (dimensionless), h the still water depth and τ the Reynolds' stress tensor. The continuity equation is

$$\partial_t\eta + \partial_{x\beta}((h+F\eta)u_\beta) + \partial_z w = 0 \qquad (2.1.2)$$

and the equation of state is

$$\rho = \rho_0(1 + \frac{g'}{g}s) \qquad 0 <= s <= 1 \qquad (2.1.3)$$

where ρ is the density of water and s is the dimensionless salinity concentration, and the reduced gravity g' is defined by

$$g' = \frac{\rho_{max} - \rho_0}{\rho_0}g$$

where ρ_{max} is the maximum density of water at the mouth of channel while ρ_0 is the density of the fresh water at the head of channel, and s is the dimensionless salinity, $0 <= s <=1$.

The scaling parameters used are as follows:

$$F = U_s/(gh)^{0.5} = \eta_s/H_s \qquad \text{long wave Froude number}$$

$$F_R = f/\omega_s = f\lambda_s^{-1}/(gH_s)^{0.5} \qquad \text{rotational Froude number}$$

$$F_D^2 = U_s^2 / (g\Delta\rho/\rho)H_s \qquad \text{densimetric long wave Froude number}$$

$$\delta = H_s \lambda_s$$

$$\lambda_s = 2\pi/L_s$$

$$L_s = (H_s g)^{1/2} T_s$$

$$T_s = 2\pi/\omega_s$$

$$z = \frac{z^* + h}{h + F\eta} = \frac{z^* + h}{H}$$

where T_s is the time scale, L_s the horizontal length scale, H_s the total water depth scale, U_s the velocity scale, ω_s the frequency scale or M2 tide frequency, g the gravitational constant, z the stretched vertical coordinate and z^* the cartesian vertical coordinate. It is noted that z^* (in dimensionless form) varies from $-h$ to $F\eta$ and z varies from 0 to 1. The equations assume dimensionless form by setting the Coriolis coefficient f, gravitational constant g and g' to unity and the total depth $H = h + F\eta$, while dimensional forms are obtained by setting the scaling parameters F, F_D, F_R to unity and $H = h + \eta$ (Hamrick, 1990).

After introducing Reynold's average procedure, it is necessary to parameterize Reynold's stress terms properly so that the equations are closed. The parameterization of Reynold's stress terms in this numerical model assumes the following form:

$$\tau_{\alpha z} = -\frac{N_v}{H} \, \partial_z u_\alpha$$

where $-\frac{N_v}{H} = S_m \frac{1^2}{H^2} |\partial_z u_\beta|$, $(\beta = 1, 2)$, S_m is a stability function which is related to stratification and 1 is the mixing length. Basically, This is an eddy viscosity parameterization which will be covered in more detail in chapter 4. As for $\tau_{\alpha\beta}$, they are rather small Reynold's stress terms and a simple parameterization is used.

$$\tau_{\alpha\beta} = N_h (\partial_{x\beta} u_\alpha + \partial_{x\alpha} u_\beta)$$

where N_h is a constant eddy viscosity coefficient. More details of turbulence parameterization will be dealt with in Chapter 4.

The instantaneous salt transport equation is an expression of the law of the conservation of mass and is presented as follows:

$$\partial_t s + \partial_{x\alpha}(u_\alpha s) + \partial_z(ws) = \partial_{x\alpha} J_\alpha + \partial_z J_z$$

where J_α and J_z are molecular diffusion fluxes and are given by Fickian diffusion Law as follows:

$$J_\alpha = - K_m \partial_{x\alpha} s$$

$$J_z = - K_m \partial_z s$$

where K_m is the molecular diffusion coefficient.

Applying Reynold's averaging procedure to the above salinity transport equation and introducing stretched coordinate and scaling analysis, the following intratidal salinity transport equation is obtained:

$$\partial_t Hs + F\partial_{x\beta}(Hu_\beta s) + F\partial_z(ws)) \qquad (2.1.4)$$

$$= (H_s \lambda_s)\partial_{x\beta}(K_h H\partial_{x\beta}s) + \partial_z(-\frac{Kv}{H}\partial_z s)$$

where the vertical turbulent mixing coefficient is scaled by $H_s^2\omega_s$ (H_s is the scale for total depth and ω_s is the scale for tide frequency, i.e. M2 tide frequency) and the horizontal turbulent mixing coefficient is scaled by $H_s^2\omega/H_s\lambda_s$. The parameterization for vertical turbulence flux and horizontal turbulence fluxes use eddy diffusivities, K_v and K_h

2.2   Two Dimensional Vertical Plane Equations

The conditions under which a two dimensional approximation of the three dimensional equation of motion is valid can be characterized in terms of two fundamental parameters. They are the Kelvin number, $K=fB/(gH_0)^{0.5}$, and the horizontal aspect ratio, $\varepsilon=\omega_s B/(gH_0)^{0.5}$ (Krauss, 1973, p.154), where B is the width of channel. The Kelvin number expresses the importance of the Coriolis terms in the narrow tidal channel and the horizontal aspect ratio measures the importance

18

of the cross-channel velocity in the cross channel momentum balance. It can be shown that if the Kelvin number and the horizontal aspect ratio are much less than unity, the Y momentum equation and all terms containing the cross channel velocity and involving differentiation with respect to y in the x-momentum equation can be neglected. For typical estuaries, these conditions are satisfied (Ianniello, 1977), and thus the following two dimensional (vertical plane) equations of momentum and continuity are obtained after some additional algebraic simplifications:

Momentum equations

$$\partial_t (Hu) + F\partial_x (Hu^2) + F\partial_z (wu) \tag{2.2.1}$$

$$= -(g)H(1 + (\frac{g'}{g})\frac{F^2}{F_D^2}s\ )\partial_x\eta + (g')\frac{F}{F_D^2}H\partial_x H(1-z)s$$

$$-(g')\frac{F}{F_D^2}H\partial_x (H\int_z^1 sdz) + \delta\partial_x (HN_H\partial_x u) + \partial_z (-\frac{Nv}{H}\ \partial_z u)$$

Continuity equation

$$\partial_t \eta + \partial_x (Hu) + \partial_z w = 0 \tag{2.2.2}$$

19

The 2-D intratidal salinity transport equation:

$$\partial_t(Hs) + F\partial_x(Hus) + F\partial_z(ws) \qquad\qquad (2.2.3)$$

$$= (H_s\lambda_s\ )\partial_x(K_hH\partial_x s) + \ \partial_z(-\frac{Kv}{H}\ \partial_z s)$$

2.3   Layered Formulation of the Equations

To reflect a distinctive anisotropic character of the estuary circulation in regard with the horizontal and vertical motion because of the hydrostatic approximation, which is justified by the shallowness of natural channels in comparison to their horizontal dimension, it is beneficial to use a layered formulation of the equations (Simoms, 1980). By means of integrating the two dimensional equations vertically from z_{k-1} to z_k the two dimensional equations are transformed to a system of coupled one dimensional equations. The dependence of the variables on the vertical coordinate is not completely eliminated, but now appears in the form of a coupling between the 1-D equations in different layers of the model. The vertical integration over each layer can ensure that the conservation character of the original differential equations and relevant volume integrals are preserved which is very important for the stability of the numerical model.

If we define the layered vertical integral variables

$$A_k = -\frac{1}{\Delta z_k} \int_{z_{k-1}}^{z_k} A\, dz \; , \qquad \Delta z_k = z_k - z_{k-1} \qquad (2.3.1)$$

the following expressions are obtained:

$$\int_{z_{k-1}}^{z_k} \partial_t(Hu)\, dz = \partial_t(H\Delta z_k u_k)$$

21

$$\int_{z_{k-1}}^{z_k} \partial_x (Hu^2) dz = \partial_x (H\Delta z_k u_k^2)$$

$$\int_{z_{k-1}}^{z_k} \partial_z (wu) \, z = (wu)_k - (wu)_{k-1}$$

$$\int_{z_{k-1}}^{z_k} (1-z) s dz = s_k \Delta z_k (1-z + \Delta z/2)$$

$$\int_z^1 s dz = \sum_{n=k}^{K} \Delta z_n s_n - s_k (z-z_{k-1}) \qquad (z_{k-1} <= z <= z_k)$$

$$(\int_z^1 s dz)_k = \Delta z_k \sum_{n=k}^{K} \Delta z_n s_n - s_k (\Delta z_k)^2 /2$$

After substituting the above layered variable expressions into the 2-D equations, the resulting layered average equations are obtained:

Layered Momentum Equation:

$$\partial_t (H\Delta z_k u_k) + F\partial_x (H\Delta z_k u_k^2) + F((wu)_k - (wu)_{k-1}) \qquad (2.3.2)$$

$$= -(g) H\Delta z_k (1 + \frac{(g')}{(g)} \frac{F^2}{F_D^2} s_k) \partial_x \eta$$

$$+ (g') \frac{F}{F_D^2} H\Delta z_k s_k (1 - z_k + \Delta z_k /2) \partial_x H + (g') \frac{F}{F_D^2} H^2 (\Delta z_k^2)/2 \; \partial x s_k$$

$$(g') \frac{F}{F_D^2} H(\Delta z_k^2)/2 (\partial_x H) s_k - (g') \frac{F}{F_D^2} H\Delta z_k \partial_x (H \sum_{n=k}^{K} \Delta z_n s_n)$$

$$+ \delta\partial_x (HN_h \Delta z_k \partial_x u_k) + (-\frac{N_v}{H} \partial_z u_k) - (-\frac{N_v}{H} \partial_z u_{k-1})$$

Layered Salt Transport Equation

$$\partial_t(Hs_k) + F\partial_x(Hus_k) + F((ws)_k - (ws)_{k-1})/\Delta z_k \qquad (2.3.3)$$

$$= (H_s\lambda_s)\partial_x(K_hH\partial_xs_k) + ((-\frac{K_v}{H})_k(s_{k+1} - s_k)/\Delta z_k$$

$$- (-\frac{K_v}{H})_{k-1}(s_k - s_{k-1})/\Delta z_{k-1})/\Delta z_k$$

3. Formulation of Numerical Scheme

3.1   Selection of Grid System

Numerical solution of the above coupled partial differential equations in most cases is obtained by using the finite difference method. Basically in this method, a set of points is introduced in the region of interest and the approximations for derivatives are used to construct a system of algebraic equations that approximate the governing partial differential equations. Dependent variables are then computed at these points and at discrete time intervals with the additional constraints that approximate the initial and the boundary conditions as required by the physics of the problem.

A uniform grid of spatially staggered variables and a forward time centered space difference scheme was used in the numerical model. Two time-level differencing is preferred because no Coriolis force is involved in the vertical plane model. The two level scheme is also much easier to implement than a three-time level scheme. The staggered grid here is especially good for vertical 2-D model since it allows more accurate phase speed for gravity waves with less calculations involved in comparison to other grid systems(Arakawa, 1972). The location of variables on the grid is shown in Figure-3.1

24

Figure 3.1 A Schematic Representation of the Computational

Grid

$z \uparrow$

z_K —

Δz_K $1,K$ I,K

z_{K-1} —

z_k —

                                  $w_{i,k}$

Δz_k $1,k$ $u_{i-1,k} \longrightarrow$ s_{ik} $\longrightarrow u_{i,k}$ I,k

z_{k-1} —

                                 $w_{i,k-1}$

z_1 —

Δz_1 $1,1$ $I,1$

z_0 — x_0 x_1 x_{i-1} x_i x_{I-1} x_I x

     Δx_1 Δx_i Δx_I
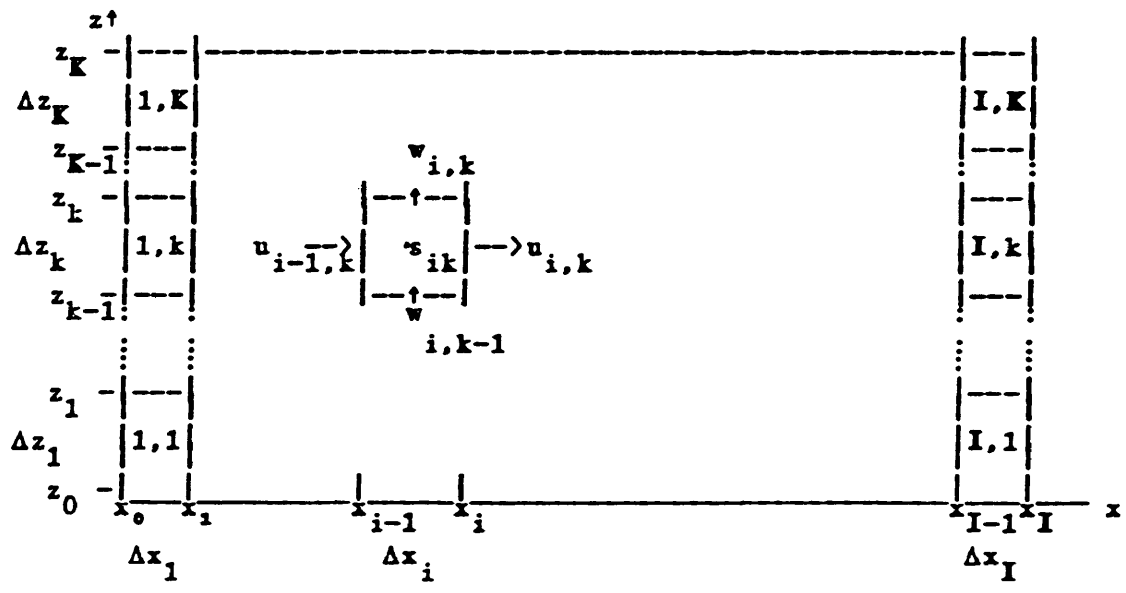
3.2   Mode Splitting

If time integration is performed explicitly, the most serious restriction on the time step comes from the phase speed of gravitational waves, and is given by CFL condition.

$$\Delta t < \frac{\Delta x}{(gh)^{0.5}} \qquad (3.2.1)$$

For $\Delta x = 3500$ M and channel depth $h = 10.0$ M, the time step $\Delta t = 350$ seconds, which is about 6 min. Since the computational time step employed in numerical models is mainly restricted by the phase speed of the fastest moving waves (i.e. surface gravity waves). The layer average equations describe both external and internal modes, but it is advantageous to reformulate the layer average equations so that internal structure of the flow is calculated more or less separated from the external mode (Simons, 1980). The **external mode** describes surface movements and vertically integrated transport while the **internal mode** determines internal velocity and mass redistribution. After the mode splitting, the pressure gradient terms in the external mode equation can be treated implicitly and the restriction of time step in the external mode comes only from the advective velocity which is in general an order of magnitude smaller than gravitational wave speed. This allows for a larger time step in the solution of the external mode equation. Also, because the characteristic phase speed in the internal mode $(gh\Delta\rho/\rho)^{1/2}$ is much smaller than that of external gravity waves, the time step in internal mode equation is no longer

restricted by the phase speed of internal waves, it is restricted by the vertical turbulent diffusion terms because of the shallow water depth. However this restriction on the time step can be removed by an implicit treatment of the vertical turbulent diffusion terms. These considerations lead to the external and internal mode equations from the layered average equations as follows:

External mode equations:

$$\partial_t(H\bar{u}) + F\partial_x\left(H\sum_{k=1}^{K}\Delta z_k u_k^2\right) = -(g)H\partial_x\eta + (\beta g)\frac{F}{F_D^2}\bar{s}H\partial_x h \qquad (3.2.2)$$

$$+ (\beta g)\frac{F}{F_D^2}H\partial_x H\sum_{k=1}^{K}\left(s_k(\Delta z_k^2) - s_k z_k \Delta z_k - \Delta z_k \sum_{n=k}^{K}\Delta z_n s_n\right)$$

$$+ (\beta g)\frac{F}{F_D^2}H^2\sum_{k=1}^{K}\left((\Delta z_k^2/2)\partial_x s_k - \Delta z_k \sum_{n=k}^{K}\Delta z_n \partial_x s_n\right) + \tau_s - \tau_b$$

The external mode equations are obtained by summing the layered average equations from 1 to K (K: the number of layers) and the $\bar{u}$ and $\bar{s}$ are defined as follows:

$$\bar{u} = \sum_{k=1}^{K} \Delta z_k u_k \qquad (3.2.3)$$

$$\bar{s} = \sum_{k=1}^{K} \Delta z_k s_k \qquad (3.2.4)$$

Internal mode equations:

$$\partial_t(H\Delta u_k) + F\partial_x(Hu_{k+1}^2 - Hu_k^2) \qquad (3.2.5)$$

27

$$+ F\left(\frac{(wu)_{k+1} - (wu)_k}{\Delta z_{k+1}}\right) - F\left(\frac{(wu)_k - (wu)_{k-1}}{\Delta z_k}\right)$$

$$= (\beta g)\frac{F}{F_D^2}(s_{k+1} - s_k)(\partial_x h - z_k \partial_x H)H$$

$$+ (\beta g)\frac{F}{F_D^2}\frac{H^2}{2}(\Delta z_{k+1}\partial_x s_{k+1} + \Delta z_k \partial_x s_k)$$

$$+ \frac{\tau_{k+1}}{\Delta z_{k+1}} - \left(\frac{1}{\Delta z_{k+1}} + \frac{1}{\Delta z_k}\right)\tau_k + \frac{\tau_{k-1}}{\Delta z_k}$$

$$+ \partial_x(HN_h \partial_x \Delta u_k)$$

The internal mode equations are obtained by subtraction of the layered average equation with index k from that with k+1 and so forth to K-1, with Δu_k mand τ_k are defined as follows:

$$\Delta u_k = u_{k+1} - u_k$$

$$\tau_k = \left(-\frac{Nv}{H}\partial_z u\right)_k = \left(\frac{Nv}{H}\right)_k \frac{\Delta u_k}{\Delta z_k} \qquad (3.2.6)$$

The continuity equation for external mode is as follows:

$$\partial_t \eta + \partial_x(\overline{Hu}) = 0 \qquad (3.2.7)$$

From the continuity equation (2.3.2) and the continuity equation for external mode (3.2.7), we can get

$$\partial_x (H(u - \bar{u})) + \partial_z w = 0 \qquad\qquad (3.2.8)$$

and after integrating (2.2.8) from z_{k-1} to z_k with respect to z, we get

$$\partial_x (H\Delta z_k (u_k - \bar{u})) + w_k - w_{k-1} = 0 \qquad\qquad (3.2.9)$$

which can be solved for w_k given w_{k-1}, $\bar{u}$ and u_k.

In summary, the pressure gradient term in the external mode equation will be treated semi-implicitly (Mesinger and Arakawa, 1976) to overcome the restriction on the length of time step. This will lead to a tridiagonal system of linear equations which can be solved for η and $\bar{u}$ very fast and efficiently. The internal mode equation will be solved implicitly in z direction to overcome the restriction on time step resulting from the vertical turbulent diffusion terms because of the instability associated with shallow water. The vertical implicit scheme will lead to a tridiagonal system of linear equations which can be solved for Δu_k and in turn u_k can be obtained from $\bar{u}$ and Δu_k. Numerical experiments show that the bottom stress term can be treated explicitly while other vertical stress terms are treated implicitly and this can be explained by the fact that bottom stress term is in essence not in a Fickian form and does not follow the restriction on time step of the other diffusion terms. In this way, a very efficient numerical scheme results and the time integration can be carried out

with a much larger time step. This will provide a solid foundation for a real time, long-term simulation of the estuary residual circulation, presumably about 45 days after the model has reached an equilibrium state.

3.3   Boundary Conditions

For a stretched vertical coordinate, the boundary conditions at the surface are

$$-\frac{N_v}{H}(\partial_z u)\ \Big|_{z=1} = \tau_s \tag{3.3.1}$$

$$-\frac{K_v}{H}(\partial_z s)\ \Big|_{z=1} = 0 \tag{3.3.2}$$

$$w\Big|_{z=1} = 0 \tag{3.3.4}$$

where τ_s is the surface wind stress and evaporation and precipitation are not considered.

Similarly, at the bottom

$$-\frac{N_v}{H}(\partial_z u)\ \Big|_{z=0} = \tau_b \tag{3.3.5}$$

$$-\frac{K_v}{H}(\partial_z s)\ \Big|_{z=0} = 0 \tag{3.3.6}$$

$$w\ \Big|_{z=0} = 0 \tag{3.3.7}$$

The bottom stress τ_b is obtained by matching the logarithmic law of the wall using the following expression:

$$\tau_b = C_D |u_b| u_b \tag{3.3.8}$$

31

where $C_D = (k/\ln(z_b/z_0)^2$, k is von Karman constant, z_0 the roughness coefficient and z_b and u_b are the grid point and corresponding velocity nearest the bottom respectively.

At the open boundaries, the sea level elevation is specified as

$$\eta_0 = \bar{\eta}_0 \sin(\omega_1 t) \qquad (3.3.9)$$

where $\bar{\eta}_0$ is the tidal amplitude and ω_1 is M_2 tide frequency or η_0 can be the sum of several tidal constituents according to the problem at hand. As for the salinity at the open boundary, during ebb, salinities are calculated using an upwind differenced advective equation, whereas during flood, the salinity is linearly interpolated for a duration of one hour and twenty minutes from its computed value at the end of ebb to a value set at the open boundary. At the upstream end of the channel, fresh water discharge velocities are specified and salinities are set to zero.

3.4 Numerical Scheme for External Mode Equation

The external mode momentum and continuity equations are presented again as follows:

$$\partial_t(H\bar{u}) + F\partial_x\left(H\sum_{k=1}^{K}\Delta z_k u_k^2\right) = -(g)H\partial_x\eta + (\beta g)\frac{F}{F_D^2}\bar{s}H\partial_x h$$

$$+ (\beta g)\frac{F}{F_D^2}H\partial_x H\sum_{k=1}^{K}\left(s_k(\Delta z_k^2) - s_k z_k \Delta z_k - \Delta z_k \sum_{n=k}^{K}\Delta z_n s_n\right)$$

$$+ (\beta g)\frac{F}{F_D^2}H^2\sum_{k=1}^{K}\left((\Delta z_k^2/2)\partial_x s_k - \Delta z_k \sum_{n=k}^{K}\Delta z_n \partial_x s_n\right) + \tau_s - \tau_b$$

$$\partial_t\eta + \partial_x(H\bar{u}) = 0$$

where $\bar{u}$ and $\bar{s}$ are defined as follows:

$$\bar{u} = \sum_{k=1}^{K}\Delta z_k u_k \qquad \text{and} \qquad \bar{s} = \sum_{k=1}^{K}\Delta z_k s_k$$

The following terms and difference operators are introduced.

$$A = F\partial_x\left(H\sum_{k=1}^{K}\Delta z_k u_k^2\right) \tag{3.4.1}$$

$$D = (g')\frac{F}{F_D^2}\bar{s}H\partial_x h + (g')\frac{F}{F_D^2}H\partial_x H\sum_{k=1}^{K}(s_k(\Delta z_k^2) \tag{3.4.2}$$

$$- s_k z_k \Delta z_k - \Delta z_k \sum_{n=k}^{K}\Delta z_n s_n))$$

$$+ (g')\frac{F}{F_D^2}H^2\sum_{k=1}^{K}\left((\Delta z_k^2/2)\partial_x s_k - \Delta z_k \sum_{n=k}^{K}\Delta z_n \partial_x s_n\right)$$

$$T = \tau_s - \tau_b \tag{3.4.3}$$

$$\Delta_x^+ f_i = \frac{f_{i+1} - f_i}{\Delta x} \qquad \text{(Forward)} \tag{3.4.4}$$

$$\Delta_x^- f_i = \frac{f_i - f_{i-1}}{\Delta x} \qquad \text{(Backward)} \tag{3.4.5}$$

$$\Delta_t^+ f^n = \frac{f^{n+1} - f^n}{\Delta t} \tag{3.4.6}$$

Treating the pressure gradient term semi-implicitly, the discretized form for the momentum equation is as follows:

$$\Delta_t^+ (\bar{H}u)_i^n + A_i = -(g)H_i(\alpha\Delta_x^+ \eta_i^{n+1} + (1-\alpha)\Delta_x^+ \eta_i^n) + D_i^n + T_i^n \tag{3.4.7}$$

The discretized form for the continuity equation is as follows:

$$\Delta_t^+ \eta^n + \alpha\Delta_x^-(\bar{H}u)_i^{n+1} + (1-\alpha)\Delta_x^-(\bar{H}u)_i^n = 0 \tag{3.4.8}$$

From the momentum equation, we can solve for $(\bar{H}u)_i^{n+1}$ and $(\bar{H}u)_{i-1}^n$ as follows:

$$(\bar{H}u)_i^{n+1} = (\bar{H}u)_i^n - \frac{\Delta t\alpha(g)}{\Delta x}H_i(\eta_{i+1}^{n+1} - \eta_i^{n+1}) \tag{3.4.9}$$

$$- \frac{\Delta t(1-\alpha)(g)}{\Delta x}H_i(\eta_i^n - \eta_i^n)$$

$$- \Delta t A_i^n + \Delta t D_i^n + \Delta t T_i^n + \Delta t R_i^n$$

34

$$(\overline{Hu})_{i-1}^{n+1} = (\overline{Hu})_{i-1}^{n} - \frac{\Delta t \alpha(g)}{\Delta x} H_{i-1}(\eta_i^{n+1} - \eta_{i-1}^{n+1}) \qquad (3.4.10)$$

$$- \frac{\Delta t(1-\alpha)(g)}{\Delta x} H_{i-1}(\eta_i^{n} - \eta_{i-1}^{n})$$

$$- \Delta t A_{i-1}^{n} + \Delta t D_{i-1}^{n} + \Delta t T_{i-1}^{n} + \Delta t R_{i-1}^{n}$$

From (2.4.8), we get the following relation for i < IM.

$$\eta_i^{n+1} + \frac{\Delta t}{\Delta x} \alpha[(\overline{Hu})_i^{n+1} - (\overline{Hu})_{i-1}^{n+1}] = \eta_i^{n} \qquad (3.4.11)$$

$$- \frac{\Delta t}{\Delta x}(1-\alpha)[(\overline{Hu})_i^{n} - (\overline{Hu})_{i-1}^{n}]$$

and for i = IM, we have

$$\eta_{IM}^{n+1} + \frac{\Delta t}{\Delta x} \alpha[Q - (\overline{Hu})_{IM-1}^{n+1}] = \eta_{IM}^{n} - \frac{\Delta t}{\Delta x}(1-\alpha)[Q - (\overline{Hu})_{IM-1}^{n}]$$

$$(3.4.12)$$

where Q = fresh water discharge per unit width. Substituting $(\overline{Hu})_i^{n+1}$

and $(\overline{Hu})_{i-1}^{n+1}$ of (2.4.9) and (2.4.10) into (2.4.11) and (2.4.12), a

tridiagonal simultaneous equation is obtained. This kind of

simultaneous equation could be solved very efficiently by a standard

routine and the whole tridiagonal system of simultaneous equations

obtained are as follows:

For i = 1,

$$(H_0 + H_1 + \frac{1}{(G)\alpha^2}(\frac{\Delta x}{\Delta t})^2)\eta_1^{n+1} - H_1\eta_2^{n+1} = H_0(\frac{(1-\alpha)}{\alpha}\eta_0^n + \eta_0^{n+1})$$

<div align="right">(3.4.13)</div>

$$+ (\frac{1}{(G)\alpha^2}(\frac{\Delta x}{\Delta t})^2 - \frac{(1-\alpha)}{\alpha}(H_1 + H_0))\eta_1^n + \frac{(1-\alpha)}{\alpha}H_1\eta_2^n$$

$$- (\frac{1}{(G)\alpha^2}(\frac{\Delta x}{\Delta t}))((\bar{H u})_1^n - (\bar{H u})_0^n) + \frac{\Delta x}{(G)\alpha}(T_1^n - T_0^n)$$

$$+ \frac{\Delta x}{(G)\alpha}(D_0^n - D_1^n)$$

For 1 < i < IM,

$$-H_{i-1}\eta_{i-1}^{n+1} + (H_{i-1} + H_i + \frac{1}{(G)\alpha^2}(\frac{\Delta x}{\Delta t})^2)\eta_i^{n+1} - H_i\eta_{i+1}^{n+1} \qquad (3.4.14)$$

$$= -\frac{1-\alpha}{\alpha}H_{i-1}^n\eta_{i-1}^n + (\frac{1}{(G)\alpha^2}(\frac{\Delta x}{\Delta t})^2 - \frac{1-\alpha}{\alpha}(H_{i-1}^n + H_i^n))\eta_i^n$$

$$+ \frac{1-\alpha}{\alpha}H_{i-1}^n\eta_{i+1}^n - (\frac{1}{(G)\alpha^2}(\frac{\Delta x}{\Delta t}))((\bar{H u})_i^n - (\bar{H u})_{i-1}^n)$$

$$+ \frac{\Delta x}{(G)\alpha}(A_i^n - A_{i-1}^n + T_i^n - T_{i-1}^n) + \frac{\Delta x}{(G)\alpha}(D_{i-1}^n - D_i^n)$$

For $i = IM$,

$$-H_{IM-1}\eta_{IM-1}^{n+1} + (H_{IM-1} + \frac{1}{(G)\alpha^2}(\frac{\Delta x}{\Delta t})^2)\eta_{IM}^{n+1} = -\frac{1-\alpha}{\alpha}H_{IM-1}^n\eta_{IM-1}^n$$

$$(3.4.15)$$

$$+ (\frac{1}{(G)\alpha^2}(\frac{\Delta x}{\Delta t})^2 - \frac{1-\alpha}{\alpha}H_{IM-1}^n)\eta_{IM}^n - (\frac{1}{(G)\alpha^2}(\frac{\Delta x}{\Delta t}))(Q - (\overline{Hu})_{IM-1}^n)$$

$$+ \frac{\Delta x}{(G)\alpha}(- A_{IM-1}^n + T_{IM}^n - T_{IM-1}^n)$$

Note that for $i = 0$, η_0^{n+1} and η_0^n are the tidal forcing terms at the mouth.

$$\eta_0^{n+1} = \overline{\eta}_0 \sin((n+1)\omega\Delta t) \quad \text{and} \quad \eta_0^n = \overline{\eta}_0 \sin(n\omega\Delta t)$$

where $\overline{\eta}_0$ is the amplitude of the tidal forcing at the mouth of the channel.

3.5 Numerical Scheme for Internal Mode Equation

Because of the shallow water depth generally associated with estuaries, the vertical turbulent diffusion terms restrict the time step if they are treated explicitly. These terms are treated semi-implicitly to remove the restriction on the time step. The vertical implicity will generally lead to a tridiagonal system of linear equations. The shear mode equation is reproduced as follows:

$$\partial_t(H\Delta u_k) + F\partial_x(Hu_{k+1}^2 - Hu_k^2) + F\left(\frac{(wu)_{k+1} - (wu)_k}{\Delta z_{k+1}}\right) - F\left(\frac{(wu)_k - (wu)_{k-1}}{\Delta z_k}\right)$$

$$= (g')\frac{F}{F_D^2}(s_{k+1} - s_k)(\partial_x h - z_k\partial_x H)H$$

$$+ (g')\frac{F}{F_D^2}\frac{H^2}{2}(\Delta z_{k+1}\partial_x s_{k+1} + \Delta z_k\partial_x s_k)$$

$$+ \frac{\tau_{k+1}}{\Delta z_{k+1}} - \left(\frac{1}{\Delta z_{k+1}} + \frac{1}{\Delta z_k}\right)\tau_k + \frac{\tau_{k-1}}{\Delta z_k}$$

$$+ \partial_x(HN_h\partial_x\Delta u_k)$$

where $\tau_k = (-\frac{Nv}{H}\partial_z u)_k$ and Δu_k is defined as follows:

$$\Delta u_k = u_{k+1} - u_k$$

Introducing the following notation

$$C = F\partial_x(Hu_{k+1}^2 - Hu_k^2) \quad (\text{ Advec. terms }) \qquad (3.5.1)$$

38

$$G = F(\frac{(wu)_{k+1} - (wu)_k}{\Delta z_{k+1}}) - F(\frac{(wu)_k - (wu)_{k-1}}{\Delta z_k}) \quad (\text{Advec. terms})$$

$$(3.5.2)$$

$$D = (g')H\frac{F}{F_D^2}(s_{k+1} - s_k)(\partial_x h - z_k \partial_x H)H \qquad (3.5.3)$$

$$+ (g')\frac{F}{F_D^2}\frac{H^2}{2}(\Delta z_{k+1}\partial_x s_{k+1} + \Delta z_k \partial_x s_k) \qquad (\text{Density term})$$

$$E = -\frac{\tau_{k+1}}{\Delta z_{k+1}} - (\frac{1}{\Delta z_{k+1}} + \frac{1}{\Delta z_k})\tau_k + \frac{\tau_{k-1}}{\Delta z_k} \quad (\text{Stress term}) \quad (3.5.4)$$

$$P = \partial_x(HN_h \partial_x \Delta u_k) \qquad (\text{Horizontal diffusion term}) \qquad (3.5.5)$$

leads to the system of equations.

$$H\Delta u_k^{n+1} - \Delta t \xi E_k^{n+1} = H\Delta u_k^n + \Delta t(1-\xi)E_k^n + \Delta t\{D_k^n - C_k^n - G_k^n + P_k^n\}$$

$$(3.5.6)$$

After many numerical experiments, it was shown that the bottom stress term τ_0 can be treated explicitly, i.e. $\tau_0 = C_D|u_1^n|u_1^n$, with the advantage that only a tridiagonal system of equations needs to be solved. If the bottom stress term τ_0 is treated implicitly, τ_0 needs to take the following form:

$$\tau_0^{n+1} = C_D|u_1|(\bar{u} - \frac{1}{K}\sum_{k=1}^{K}(K - k)\Delta u_k^{n+1})$$

which leads to a bordered tridiagonal system of equations after substituting it into E_k^{n+1}. The bordered tridiagonal equations are more complicated to solve than tridiagonal system of equations.

Thus for $k = 1$, we have

$$E_1^{n+1} = \frac{\tau_2^{n+1}}{\Delta z_2} - (\frac{1}{\Delta z_2} + \frac{1}{\Delta z_1})\tau_1^{n+1} \qquad (3.5.7)$$

$$E_1^{n} = \frac{\tau_2^{n}}{\Delta z_2} - (\frac{1}{\Delta z_2} + \frac{1}{\Delta z_1})\tau_1^{n} + (\frac{1}{1-\xi})\frac{\tau_0^{n}}{\Delta z_1} \qquad (3.5.8)$$

where τ_0 is the bottom stress which has the form of

$$\tau_0^{n} = C_D |u_1^{n}| u_1^{n} \qquad (3.5.9)$$

$$\tau_k^{n} = (\frac{Nv}{H})_k^{n}(\Delta u_k^{n}/\Delta z) \qquad KM > k > 1 \qquad (3.5.10)$$

$$\tau_k^{n+1} = (\frac{Nv}{H})_k^{n}(\Delta u_k^{n+1}/\Delta z) \qquad KM > k > 1 \qquad (3.5.11)$$

After substituting τ_0 and τ_k into E_1^{n+1} and E_1^{n}, we get

$$E_1^{n} = \frac{1}{\Delta z_2}(\frac{N_v}{H})_2^{n}\frac{\Delta u_2^{n}}{\Delta z_2} - (\frac{1}{\Delta z_2} + \frac{1}{\Delta z_1})(\frac{N_v}{H})_1^{n}\frac{\Delta u_1^{n}}{\Delta z_1} \qquad (3.5.12)$$

40

$$+(-\frac{1}{1-\xi})\frac{1}{\Delta z_1}C_D|u_1^n|u_1^n$$

$$E_1^{n+1} = \frac{1}{\Delta z_2}(\frac{N_v}{H})_2^n\frac{\Delta u_2^{n+1}}{\Delta z_2} - (\frac{1}{\Delta z_2} + \frac{1}{\Delta z_1})(\frac{N_v}{H})_1^n\frac{\Delta u_1^{n+1}}{\Delta z_1}$$

For $k = 2$, $KM-2$, we have

$$E_k^n = \frac{1}{\Delta z_{k+1}}(\frac{N_v}{H})_{k+1}^n\frac{\Delta u_{k+1}^n}{\Delta z_{k+1}} - (\frac{1}{\Delta z_{k+1}} + \frac{1}{\Delta z_k})(\frac{N_v}{H})_k^n\frac{\Delta u_k^n}{\Delta z_k} \qquad (3.5.13)$$

$$+ \frac{1}{\Delta z_k}(\frac{N_v}{H})_{k-1}^n\frac{\Delta u_{k-1}^n}{\Delta z_k}$$

$$E_k^{n+1} = \frac{1}{\Delta z_{k+1}}(\frac{N_v}{H})_{k+1}^n\frac{\Delta u_{k+1}^{n+1}}{\Delta z_{k+1}} - (\frac{1}{\Delta z_{k+1}} + \frac{1}{\Delta z_k})(\frac{N_v}{H})_k^n\frac{\Delta u_k^{n+1}}{\Delta z_k}$$

$$+ \frac{1}{\Delta z_k}(\frac{N_v}{H})_{k-1}^n\frac{\Delta u_{k-1}^{n+1}}{\Delta z_k} \qquad (3.5.14)$$

For $k = KM-1$, τ_{KM-1} is just the surface wind stress and we have

$$E_{KM-1}^n = \tau_{KM-1}(\text{Surf. stress})/\Delta z_{KM} \qquad (3.5.15)$$

$$- (\frac{1}{\Delta z_{KM}} + \frac{1}{\Delta z_{KM-1}})(\frac{N_v}{H})_{KM-1}^n\frac{\Delta u_{KM-1}^n}{\Delta z_{KM-1}} + \frac{1}{\Delta z_{KM-1}}(\frac{N_v}{H})_{KM-2}^n\frac{\Delta u_{KM-2}^n}{\Delta z_{KM-1}}$$

$$E_{KM-1}^{n+1} = \tau_{KM}(\text{Surf. stress})/\Delta z_{KM} \qquad (3.5.16)$$

41

$$- (-\frac{1}{\Delta z_{KM}} + -\frac{1}{\Delta z_{KM-1}})(-\frac{N_v}{H})^n_{KM-1} \frac{\Delta u^{n+1}_{KM-1}}{\Delta z_{KM-1}} + \frac{1}{\Delta z_{KM-1}} (-\frac{N_v}{H})^n_{KM-2} \frac{\Delta u^{n+1}_{KM-2}}{\Delta z_{KM-1}}$$

Substituting (3.5.7) through (3.5.16) into (3.5.6), a tridiagonal system of linear simultaneous equation is obtained.

For $k = 1$,

$$(H^{n+1} + \xi\frac{\Delta t}{\Delta z_1}(-\frac{1}{\Delta z_2} + -\frac{1}{\Delta z_1})(-\frac{Nv_1}{H})\ )\Delta u^{n+1}_1 - \xi\frac{\Delta t}{\Delta z_2}(-\frac{Nv_2}{H})\Delta u^{n+1}_2 \quad (3.5.17)$$

$$= H^n\Delta u^n_1 + (1-\xi)\Delta tE^n_1 + \Delta tD^n_1 - \Delta tC^n_1 - \Delta tG^n_1 + \Delta tP^n_1$$

For $1 < k < KM-2$,

$$- \frac{\xi\Delta t}{\Delta z_k}(-\frac{Nv_{k-1}}{H})^n \frac{\Delta u^{n+1}_{k-1}}{\Delta z_{k-1}} + (H^{n+1} + -\frac{\xi\Delta t}{\Delta z_k}(-\frac{1}{\Delta z_{k+1}} + -\frac{1}{\Delta z_k})(-\frac{Nv_k}{H})^n)\Delta u^{n+1}_k$$

$$- \frac{\xi\Delta t}{\Delta z_{k+1}}(-\frac{Nv_{k+1}}{H})^n \frac{\Delta u^{n+1}_{k+1}}{\Delta z_{k+1}} = H^n\Delta u^n_k + \Delta t(1-\xi)E^n_k + \Delta tD^n_k \quad (3.5.18)$$

$$- \Delta tC^n_k - \Delta tG^n_k + \Delta tP^n_k$$

For $k = KM - 1$,

$$- \frac{\xi \Delta t}{\Delta z_{KM-1}} \left(\frac{Nv_{KM-2}}{H} \right)^n \frac{\Delta u_{KM-2}^{n+1}}{\Delta z_{KM-2}} \qquad\qquad (3.5.19)$$

$$+ \left(H^{n+1} + \frac{\xi \Delta t}{\Delta z_K} \left(\frac{1}{\Delta z_{KM}} + \frac{1}{\Delta z_{KM-1}} \right) \left(\frac{Nv_{KM-1}}{H} \right)^n \right) \Delta u_{KM-1}$$

$$= H^n \Delta u_{KM-1} + \Delta t (1-\xi) E_{KM-1}^n + \Delta t \xi \tau_{KM} (\text{surf. stress}) / \Delta z_{KM}$$

$$+ \Delta t D_1^n - \Delta t C_1^n - \Delta t G_1^n + \Delta t P_1^n$$

3.6 Numerical Scheme for Layered Salt Transport Equation

The layered salt transport equation is as follows:

$$\partial_t(Hs_k) + F\partial_x(Hus_k) + F((ws)_k - (ws)_{k-1})/\Delta z_k \qquad (3.6.1)$$

$$= (H\lambda)\partial_x(K_h H\partial_x s_k) + (J_k - J_{k-1})/\Delta z_k$$

where $J_k = (-\frac{Kv}{H})_k(s_{k+1} - s_k)/\Delta z_k.$ $\qquad (3.6.2)$

As in the momentum equations, vertical turbulent diffusion presents the most serious restriction on the time step for the salt transport equation. The vertical salinity diffusion is to be treated semi-implicitly just like the vertical momentum flux terms in the internal mode equation. Setting Δz_k as a constant Δz, the numerical scheme for the salt transport equation is as follows:

$$H^{n+1}s_k^{n+1} - H^n s_k^n = -\frac{\Delta t}{\Delta z}(\gamma(J_k^{n+1} - J_{k-1}^{n+1}) + (1-\gamma)(J_k^n - J_{k-1}^n)) \quad (3.6.3)$$

$$- \Delta t(A_k^n + B_k^n + C_k))$$

$$A_k = F\partial_x(Hus_k) \qquad (3.6.4)$$

$$B_k = F((ws)_k - (ws)_{k-1})/\Delta z_k \qquad (3.6.5)$$

$$C_k = (H\lambda)\partial_x(K_h H\partial_x s_k) \qquad (3.6.6)$$

Rearranging terms at level n+1 , the following is obtained:

$$H^{n+1}s_k^{n+1} - \frac{\Delta t}{\Delta z}(\gamma(J_k^{n+1} - J_{k-1}^{n+1}) = H^n s_k^n + \frac{\Delta t}{\Delta z}(1-\gamma)(J_k^n - J_{k-1}^n)$$

$$+ \Delta t (A_k^n + B_k^n + C_k^n) \qquad (3.6.7)$$

where the vertical turbulent flux of salt J_k is

$$J_k = (-\frac{Kv}{H})_k (s_{k+1} - s_k)/\Delta z_k$$

If we substituting J_k to (3.6.7), using the boundary conditions of J_0 = 0 and J_{KM} = 0 and after some algebraic manipulations, the following simultaneous linear equations, with a tridiagonal matrix of coefficients, is obtained.

For $k = 1$,

$$(H^{n+1} + \frac{\Delta t}{\Delta z^2}\gamma(-\frac{Kv}{H})_1^n s_1^{n+1} - \frac{\Delta t}{\Delta z^2}\gamma(-\frac{Kv}{H})_1^n s_2^{n+1} = H^n s_1^n \qquad (3.6.8)$$

$$+ \frac{\Delta t}{\Delta z^2}(1-\gamma)(-\frac{Kv}{H})_1^n(s_2^n - s_1^n) - \Delta t(A_1^n + B_1^n)$$

For $k > 1$ and $< KM$,

$$- \frac{\Delta t}{\Delta z^2}\gamma(-\frac{Kv}{H})_k^n s_{k-1}^{n+1} + (H^{n+1} + \frac{\Delta t}{\Delta z^2}\gamma((-\frac{Kv}{H})_k^n + (-\frac{Kv}{H})_{k-1}^n)s_k^{n+1} \qquad (3.6.9)$$

$$- \frac{\Delta t}{\Delta z^2}\gamma(-\frac{Kv}{H})_k^n s_{k+1}^{n+1} = H_k^n s_k^n + \frac{\Delta t}{\Delta z^2}(1-\gamma)(-\frac{Kv}{H})_k^n(s_{k+1}^n - s_k^n)$$

$$- \frac{\Delta t}{\Delta z^2}(1-\gamma)(-\frac{Kv}{H})_{k-1}^n(s_k^n - s_{k-1}^n) - \Delta t(A_k^n + B_k^n + C_k^n)$$

For k = KM,

$$-\frac{\Delta t}{\Delta z^2}\gamma\left(-\frac{Kv}{H}\right)_k^n s_{KM-1}^{n+1} + \left(H^{n+1} + \frac{\Delta t}{\Delta z^2}\gamma\left(\left(-\frac{Kv}{H}\right)_{KM-1}^n\right)s_{KM}^{n+1} = H_{KM}^n s_{KM}^n$$

$$- \frac{\Delta t}{\Delta z^2}(1-\gamma)\left(-\frac{Kv}{H}\right)_{KM-1}^n\left(s_{KM}^n - s_{KM-1}^n\right) - \Delta t\left(A_{KM}^n + B_{KM}^n\right) \qquad (3.6.10)$$

4. Parameterization of Turbulence

4.1 What is a Turbulence Model?

Turbulence is an eddying, highly random, unsteady, and always three-dimensional motion with a wide spectrum of eddy sizes and a corresponding spectrum of fluctuation frequencies. Turbulence occurs in a variety of flows, e.g. the mixing of cream in a coffee cup, the dispersal of pollutants in the atmosphere, the formation of galaxies in the early universe and the flows in an estuary.

In spite of all the advances in computer technology, it is still very difficult to resolve small-scale turbulent motion in a numerical calculation. The exact equations describing every detail of the turbulent fluctuations are believed to be the Navier-Stokes equations and the numerical procedures are available to solve these equations in principle, but the storage capacity and speed required are still too high to be practical by present day computers. Hence calculations can only be carried out when the motion that can not be resolved is accounted for by a model. In most situations, engineers are interested only in the mean quantity of motion, and the turbulent fluctuations are removed completely by implementing the Reynolds average procedure, The resulting turbulent stress terms (i.e. Reynolds stress) and turbulent mass or heat flux terms are then accounted for by a suitable parametric representation of the effect of these

turbulent terms on the average motion. This representation is usually referred to as a turbulence model.

4.2   Mathematical Formulation of Turbulence Model

The formulation of a turbulence model for estuaries is especially difficult because of the influence of unsteadiness and buoyancy on turbulence. The simplest turbulence models employ turbulent viscosity and diffusivity concepts in an analogy to molecular viscous stresses and fluxes in laminar flow. The important difference is that the turbulent viscosity and diffusivity are no longer fluid properties like their molecular counterparts but depend strongly on the state of turbulence and flow. The formulation of a turbulence model becomes a problem of determining the distribution of turbulent viscosity and diffusivity in the flow field. A typical example is the Prandtl mixing length model which does give reasonable results for estuarine circulation when combined with several empirical relations to take into account the influence of buoyancy characterized by the gradient Richardson number. The need to adjust the empirical constants for different estuaries is one of the major drawbacks of the mixing length model. This can be traced back to the basic assumption of the model which asserts that turbulence is in a state of local equilibrium everywhere, and neither the transport of turbulence nor the historical effects are taken into account in the Prandtl mixing length model. Since estuarine circulation is very complicated, involving unsteady flows and shear layers with flow reversal, the parameterization of turbulence is especially important to the accuracy of estuarine numerical models (ASCE, 1988).

48

More complicated turbulence models solve transport equations for the Reynolds stress and the turbulent heat or mass flux and thus take into account transport and history effects. This kind of turbulence model, i.e. stress/flux model, simulates the physical processes more realistically because more physics is considered in the model. The Reynolds stress/flux transport equations can be derived in exact form from Navier-Stokes and mass transport equations and they will automatically introduce terms accounting for buoyancy, rotation, and other special effects. This is important not only for the full Reynolds stress/flux transport model but also for its simplified form, the algebraic stress/flux model, which will be mentioned below. The stress/flux transport equations in exact form contain higher order correlations which must be modeled to obtain a closed equation. This is generally achieved by introduction of several closure hypotheses based on physics considerations. One of these is the energy redistribution hypothesis of Rotta (1951) which concerns the modeling of the correlations between the fluctuating pressure and other fluctuating variables such as velocity and mass concentration, and the other is the isotropic local small-scale dissipation hypothesis of Kolmogorov (1942). Third moments (triple correlations) can be modeled as down-gradient type diffusion terms but are sometimes simply neglected completely (Mellor and Yamada, 1974, 1982). Since in general three-dimensional flow, there are six components of the Reynolds stresses and three components of scalar flux, plus one equation for variance, a turbulence model employing the stress/flux transport equations would therefore require the solution of ten partial

49

differential equations numerically. This is not a trivial task even with modern numerical schemes and computers and definitely not economical. Thus it is very important to find ways to simplify these transport equations so that they might be reduced to algebraic expressions but still retain most of their basic physics, including the buoyancy effects.

4.3   Level-2 Turbulence Model

The level of a turbulence model necessary to obtain accurate predictions of the mean flow quantities certainly depends on the relative importance of the turbulence transport terms in the equations. A hierachy of turbulence closure models for planetary boundary layers are presented by Mellor and Yamada (1974). The most complicated full mean Reynolds stress model equations are classified as the level-4 model. This, with regard to the relative ordering of all the terms in the full mean Reynolds stress model, can be simplified to level-3, level-2 and level-1 models. For example, many flows evolve so slowly that the rate of change of both advection and diffusion terms (third moments) of the turbulent stresses and fluxes can be justifiably neglected all together as an approximation to the full equation (level-4). The resulting algebraic (level-2) models are sufficiently accurate in many cases. The Reynold stress and salt flux relations for the level-2 model in two dimensions, after Mellor and Yamada (1975, 1984), are presented as follows:

(Note: lower case letters now represent fluctuating variable and upper case letters ensemble mean variables to the end of Chapter 4.)

$$\overline{w^2}: \quad 2g'(1 - \tfrac{2}{3}C_2)\overline{ws} - \frac{q}{3l_1}(\overline{w^2} - \frac{q^2}{3}) - \frac{2}{3}\frac{q^3}{\lambda_1} = 0 \qquad (4.3.1)$$

$$\overline{uw}: \quad -(\overline{w^2} - C_1q^2)\frac{\partial U}{\partial z} + g'(1-C_2)\overline{us} - \frac{q}{3l_1}\overline{uw} = 0 \qquad (4.3.2)$$

$$\overline{us}: \quad -\overline{uw}\frac{\partial S}{\partial z} - \overline{ws}\frac{\partial U}{\partial z} - \frac{q}{3l_2}\overline{us} = 0 \qquad (4.3.3)$$

$$\overline{ws}: \quad -\overline{w^2}\frac{\partial S}{\partial z} + g'(1-C_3)\overline{s^2} - \frac{q}{3l_2}\overline{ws} = 0 \qquad (4.3.4)$$

$$\overline{s^2}: \quad -\overline{ws}\frac{\partial S}{\partial z} - \frac{q}{\lambda_2}\overline{s^2} = 0 \qquad (4.3.5)$$

$$q^2: \quad -\overline{uw}\frac{\partial U}{\partial z} + g'\overline{ws} - \frac{q^3}{g_1} = 0 \qquad (4.3.6)$$

where u, w, s are fluctuating components of the corresponding ensemble mean quantities, U, W, S, respectively, g is the acceleration of gravity, C_1, C_2, and C_3 are empirical constants and l_1, l_2, λ_1 and λ_2 are length scales which are assumed to be proportional to each other, i.e.

$$l_1, \; l_2, \; \lambda_1, \; \lambda_2 = (A_1, A_2, B_1, B_2)l \; . \qquad (4.3.7)$$

The proportionality constants A_1, A_2, B_1, B_2 are assumed to be independent of the stratification. The numerical values for the empirical constants are obtained from laboratory experiments under neutral conditions. All mean quantities are treated as known and the

solutions are expressed in terms of a stability parameter R_f and q,

where $q^2 = 0.5*(\overline{u^2} + \overline{w^2})$. The flux Richardson number

$$R_f = \frac{g'\overline{ws}}{\overline{uw}(\partial U/\partial z)} \tag{4.3.8}$$

seems to be the most appropriate stability parameter .

After some algebraic manipulations the solutions to (4.3.1)-(4.3.6) may be expressed as (Yamada, 1975):

$$q^2 = B_1 l^2 (-\frac{\partial U}{\partial z})^2 (1-R_f) S_m \tag{4.3.9}$$

$$\overline{w^2} = [-\frac{1}{3} - 2\frac{A_1}{B_1} - 6\frac{A_1}{B_1}(1 - \frac{2}{3}C_2)\frac{R_f}{1-R_f}] q^2 \tag{4.3.10}$$

$$-\overline{uw} = l q S_m (\partial U/\partial z) = K_m (\partial U/\partial z) \tag{4.3.11}$$

$$-\overline{ws} = l q S_h (\partial S/\partial z) = K_h (\partial S/\partial z) \tag{4.3.12}$$

The terms S_m and S_h are given by

$$S_m = \frac{A_1}{B_1}(B_1 + 12A_1(1-C_2) + 3B_2(1-C_3))$$

$$*\{\frac{B_1(1-3C_1) + 12A_1(1-C_2) + 9A_2(1-C_2)}{B_1 + 3A_1(1-C_2) + 3B_2(1-C_3)}\}$$

$$* \frac{(R_{fc} - R_f)}{(1 - R_f)} \frac{(R_{f1} - R_f)}{(R_{f2} - R_f)} \tag{4.3.13}$$

$$S_h = \frac{A_2}{B_1}(B_1 + 12A_1(1-C_2) + 3B_2(1-C_3)) \qquad (4.3.14)$$

$$* \frac{(R_{fc} - R_f)}{(1 - R_f)}$$

where

$$R_{fc} = \frac{B_1 - 6A_1}{B_1 + 12A_1(1-C_2) + 3B_2(1-C_3)} \qquad (4.3.15)$$

$$R_{f1} = \frac{B_1(1-3C_1) - 6A_1}{B_1(1-3C_1) + 12A_1(1-C_2) + 9A_2(1-C_2)} \qquad (4.3.16)$$

$$R_{f2} = \frac{B_1 - 6A_1}{B_1 + 3A_1(1-C_2) + 3B_2(1-C_3)} \qquad (4.3.17)$$

The turbulence intensity, q, is obtained from the equilibrium condition as follows:

$$q = B_1^{0.5} 1|\partial_z U|(1-R_f)^{0.5} S_m^{0.5} \qquad (4.3.18)$$

At neutral conditions the flux Richardson number R_f is zero and we have:

$$S_h^n = \frac{A_2}{B_1}(B_1 - 6A_1) \qquad (4.3.19)$$

$$S_m^n = \frac{A_1}{B_1}(B_1(1-3C_1) - 6A_1) \qquad (4.3.20)$$

$$K_m^n = q1S_m^n = (A_1/B_1)^{3/2}(B_1(1-3C_1) - 6A_1)^{3/2} B_1^{0\sim5} 1^2 |\partial_z U| \qquad (4.3.21)$$

53

which is in a mixing length form. Since it is at neutral condition, S_m^n should be equal to 1, so we have:

$$\frac{A_1^3}{B_1^2}(B_1(1-3C_1) - 6A_1)^3 = 1 \quad \text{i.e.}$$

$$A_1^3 B_1(1 - 3C_1 - 6\frac{A_1}{B_1})^3 = 1, \quad (4.3.22)$$

and this gives C_1 in terms of A_1 and B_1.

Also under neutral conditions, we have:

$$S_m^n q l(\partial_z U)^2 = q^3/B_1 l \quad \text{and from which}$$

$$\frac{K_m^n * q^3}{B_1 l} = K_m^n * S_m^n q l(\partial_z U)^2 = K_m^n(\partial_z U) * K_m^n(\partial_z U) = |\tau_{xz}^n|^2 \quad \text{i.e.}$$

$$\frac{S_m^n * q^4}{B_1} = |\tau_{xz}^n|^2 \quad (4.3.23)$$

Substituting the expression of S_m^n into the above relation, we have

$$A_1(1-3C_1-6\frac{A_1}{B_1})\frac{1}{B_1} = \frac{|\tau_{xz}|^2}{q^4} \quad (4.3.24)$$

Using (4.3.22), we get

$$\frac{1}{B_1^{4/3}} = \frac{|\tau_{xz}|^2}{q^4} \quad , \text{ and so}$$

$$B_1 = \left(\frac{q}{|\tau_{xz}|^{1/2}} \right)^3 , \qquad\qquad (4.3.25)$$

which gives B_1 as the ratio of the neutral equilibrium total kinetic

energy to stress.

Also under neutral conditions, $\overline{w^2}$ becomes:

$$\overline{w^2} = \left[\frac{1}{3} - 2\frac{A_1}{B_1} \right] q^2 = \frac{q^2}{3} + \frac{A_1 l}{q} \left(- \frac{2q^3}{B_1 l} \right) \quad \text{which is}$$

$$\frac{\overline{w^2}}{q^2} = \frac{1}{3} - 2\frac{A_1}{B_1} \quad \text{and after some manipulations we can get}$$

$$\frac{A_1}{B_1} = \frac{1}{6} - \frac{1}{2}\frac{\overline{w^2}}{q^2} \qquad\qquad (4.3.26)$$

which gives A_1 from B_1 and $\dfrac{\overline{w^2}}{q^2}$.

The above calculations show clearly that all empirical

constants can be obtained from laboratory measurements under the

condition of neutral flow. This is one of the advantages of the

Mellor—Yamada level-2 turbulence model used in this work because there

is no need for users to tune the empirical constants for different

estuaries.

One aspect peculiar to estuaries is the large horizontal extent of the flow compared with the extent in the vertical direction. As a consequence, gradients of mean-flow quantities in the horizontal directions are usually small compared with those in the vertical direction. Since the turbulent transport in a certain direction can be assumed to be closely related to the gradient of the transported quantity in that direction, horizontal turbulent transport is generally much smaller than the vertical turbulent transport. In particular, as is shown in the scaled momentum equation, horizontal turbulent transport is usually small compared with other terms and therefore these terms are neglected. However, the horizontal turbulent diffusion terms in the salt transport equation cannot be neglected (Rodi, 1978), in fact they affect the horizontal distribution of salt. But since the horizontal gradients of the mean flow quantities are small, a refined simulation of these is not necessary. In addition, numerical diffusion always exists and is not distinguishable, thus a relatively crude model with a constant turbulent diffusivity is used and it appears to be sufficient to simulate the horizontal turbulent transport.

In contrast to horizontal transport, the vertical turbulent transport of momentum and salt is always important if estuaries are not vertically fully mixed. Vertical turbulent transport merits special attention.

For the 2-D vertical turbulence model:

$$\tau_{xz} = \frac{N_v}{H} \partial_z U \qquad (4.3.27)$$

$$\frac{N_v}{H} = S_m * (-\frac{1}{H})^2 * |\partial_z U| \qquad (4.3.28)$$

$$\frac{K_v}{H} = S_h (-\frac{1}{H})^2 * |\partial_z S| \qquad (4.3.29)$$

in which l is the mixing length and S_m and S_h are stability functions of the gradient Richardson Numbers. The values of the stability functions could be obtained by the following formula which is derived from the algebraic stress/flux model above

$$S_m = \left\{ \frac{(1-R_{fc}^{-1}*R_f)*(1-R_{f1}^{-1}*R_f)}{(1-R_f)^{1.5}*(1-R_{f2}^{-1}R_f)} \right\}^{1.5} \qquad (4.3.30)$$

$$S_h = \frac{1}{P_r^N} \left\{ \frac{(1-R_{fc}^{-1}*R_f)^3*(1-R_{f1}^{-1}*R_f)}{(1-R_f)^2*(1-R_{f2}^{-1}*R_f)} \right\}^{0.5} \qquad (4.3.31)$$

where R_f is the Richardson flux number, which is related to the gradient Richardson number R_i by

$$R_f = 0.5 * \{ R_{f1} + R_i*R_{f1}*R_{f2}^{-1} - ((R_{f1}+R_i*R_{f1}*R_{f2}^{-1})^2 - 4*R_{f1}*R_i)^{0.5} \} \qquad (4.3.32)$$

where R_{fc}, R_{f1} and R_{f2} are given by the empirical constants A_1, B_1, A_2, B_2, C_1, while C_2 and C_3 are zero.

$$R_{fc} = \frac{B_1 - 6A_1}{B_1 + 12A_1 + 3B_2} \tag{4.3.33}$$

$$R_{f1} = \frac{B_1(1-3C_1) - 6A_1}{B_1(1-3C_1) + 12A_1 + 9A_2} \tag{4.3.34}$$
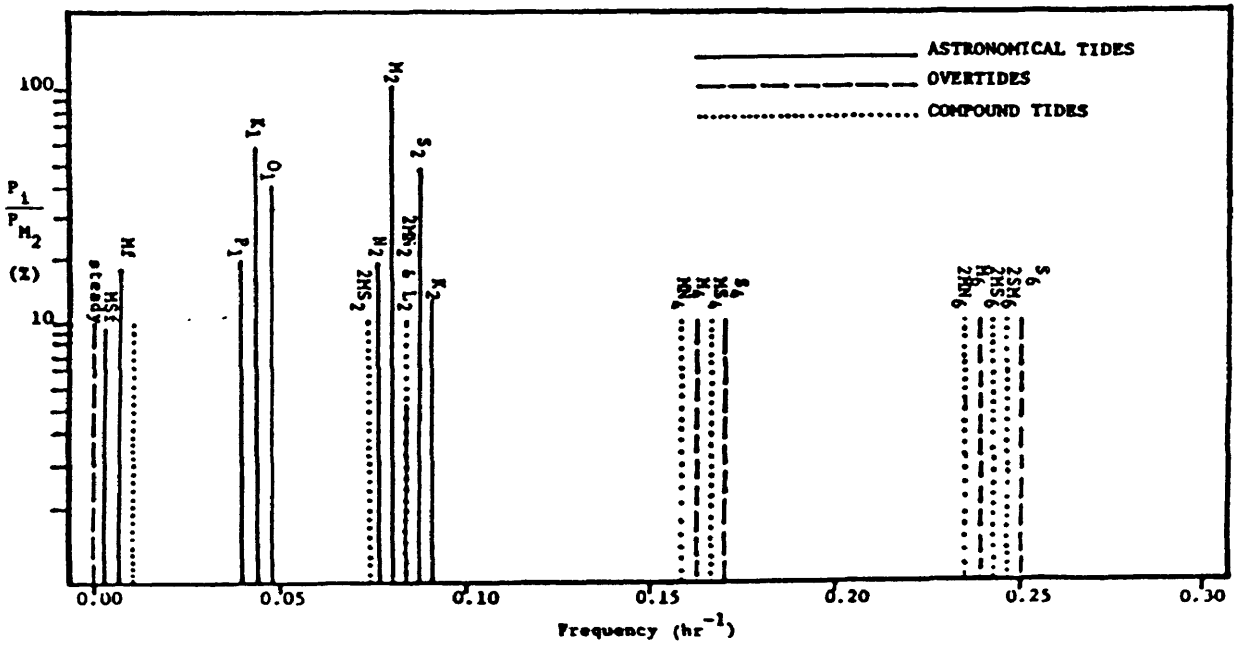
$$R_{f2} = \frac{B_1 - 6A_1}{B_1 + 3A_1 + 3B_2} \tag{4.3.35}$$

5. Analysis of Model Output

5.1   Fourier Harmonic and Least Squares Harmonic Analysis

Tides are the result of complex gravitational interactions among the moon, the sun and the oceans. For shallow water tides, non-linear effects, such as the finite amplitude of the tide (compared to the overall depth), bottom friction and convective acceleration become significant and cannot be neglected. Shallow water tides may be classified as either overtides or compound tides. Overtides result from the effect of non-linear interactions by only a single astronomical component. The frequencies associated with the overtides are exact multiples of the frequencies of the astronomical tidal components which generate them. Compound tides result from the non-linear interaction between two astronomical constituents, and their associated frequencies correspond to sums and differences of the astronomical tides which generate them (Westerink, 1985). Residual circulation corresponds to both zero frequency circulation resulting from an overtide type interaction and very low frequency compound tides produced by two major tides closely spaced in frequency (e.g. M2 and N2). Because of these two different mechanisms for generating tidal harmonics in shallow water, tidal components may exist throughout a wide range of frequencies, may be extremely closely spaced, and are, in general, **irregularly** distributed (Figure 5.1).

Figure 5.1 Schematic of Major Astronomical and Shallow Water

Tides (After Westerink, et al. 1985)

$\frac{P_1}{P_{M_2}}$

(%)

100

10

M2

K1

O1

S2

P1

N2

2MS2 & L2

2MS2

K2

steady

3SM

3M

SA

M4

MS4

MN4

S6

2SM6

2MS6

M6

2MN6

0.00   0.05   0.10   0.15   0.20   0.25   0.30

Frequency (hr^{-1})

A variety of standard Fourier harmonic analysis procedures can be applied to convert signals from the time domain to the frequency domain. Since all standard Fourier procedures operate with multiple of some base frequency, it is naturally quite suitable for examining one major astronomical tide and its overtides. For compound tides which are not integer multiple of some base frequency, however, an extremely small base frequency step may be required to extract the frequency components desired. Because of this very small frequency step, a very large number of frequencies will be processed, most of which have no associated tidal energy. In Fourier analysis procedures, time history record lengths and the total number of time sampling points increase inversely with respect to the frequency step. Hence, the finer the desired frequency resolution, the larger the amount of numerical operations required to obtain the frequency resolution needed to separate important tidal components. Consequently Fourier analysis procedures are not quite adequate for filtering the output from an estuary numerical model with compound tide components.

A very attractive alternative to standard Fourier analysis procedure is the least squares harmonic analysis method (Westerink,1985). This method implements a common least squares error minimization procedure which uses a harmonic series as the fitting function. The harmonic series only contains frequencies which are known to exist in the time history record. The method is able to extract extremely closely and irregularly spaced frequency information, yet the number of time history sampling points required is only equal to twice the number of frequencies contained in the time

61

history record. The almost infinite frequency resolution and the extremely low number of required time history sampling points make the least squares method the optimal choice for the analysis of the output from the numerical model and the extraction of the residual currents.

Given a time history record with values $f(t_i)$ at time sampling points t_i, $i = 1, N$ and with known frequency content ω_j, $j = 1, M$, the following harmonic series is used as a fitting function for the least squares procedure:

$$g(t) = \sum_{j=1}^{M} [a_j \cos\omega_j t + b_j \sin\omega_j t] \qquad (5.1.1)$$

where a_j, b_j are the unknown harmonic coefficients. The squared error between the sampling points and the fitting function is:

$$E = \sum_{i=1}^{N} |f(t_i) - g(t_i)|^2 \qquad (5.1.2)$$

$$= \sum_{i=1}^{N} [\sum_{j=1}^{M} (a_j \cos\omega_j t + b_j \sin\omega_j t) - f(t_i)]^2$$

Setting the partial derivatives of E with respect to each of the coefficients a_j and b_j to zero to accomplish error minimization, a complete set of 2M simultaneous linear equations result:

$$M_{lsq} A = S_{lsq} \qquad (5.1.3)$$

where:

M_{lsq} is the least squares (LSQ) matrix

A   is the vector of unknown coefficients

S_{lsq} is the LSQ signal vector. (Westerrink, 1985)

Steady state components in the signals being analysed are simply the arithmetic mean of the time history, so ω_j need not include the zero frequency. Furthermore, the harmonic least square method does not have the matrix ill conditioning problems because the matrix M_{lsq} is diagonally dominant due to the square of the diagonal summation terms, while other terms in the matrix are still of the same order of magnitude due to the property of the sine and cosine functions.

For a time history signal for which the entire frequency content is both known and used in the harmonic fitting series, the number of time sampling points required to find the precise components equals twice the number of frequencies. But the signal generated by the non-linear terms are such that energy is transferred indefinitely to overtide and compound tide frequencies and the number of frequencies generated increases exponentially. In practice, it is not possible to include all the frequencies generated in the fitting function and it is not necessary to include them all because the amount of energy transferred to new frequencies becomes increasingly insignificant as they appear. So the harmonic series must be truncated somewhere, which establishes an order of accuracy for the harmonic analysis. Thus the number of time history sampling points must be increased to correct the aliasing problem which depends on how many

frequencies are neglected and their associated energy levels. There will always be some compromise between the number of sampling frequencies included and the number of time sampling points required. In the case of M2 and N2 tidal forcing, five sampling frequencies are included, i.e. $M_2 - N_2$, N_2, M_2, $2M_2$, $2N_2$.

5.2 Computation of the Mean Mass Transport

The slowly varying mean mass transport field and depth field

$$u_1 \ , \ w_1 \ , \ \langle \ K_v \ \rangle$$

must be determined from the instantaneous fields

$$u \ , \ w \ , \ K_v$$

by the following relations, (Hamrick, 1990)

$$u_1 = \langle \ u_1 \ \rangle + \frac{\langle \eta_0 u_0 \rangle}{h} - \frac{1}{h} (\ \partial_z B_y) \tag{5.2.1}$$

$$w_1 = \langle \ w_1 \ \rangle + \partial_x B_y \tag{5.2.2}$$

$$\langle \ K_{v1} \rangle = \langle \ K_v \ \rangle \tag{5.2.3}$$

$$B_y = \langle \ w_0 \int u_0 dt \ \rangle \tag{5.2.4}$$

in which

    u: x velocity component

    u_0: u-$\langle u \rangle$ is short-term or high pass filtered component of u

$\langle u_1 \rangle$: long-term or Eulerian residual transport velocity

$\dfrac{\langle \eta_0 u_0 \rangle}{h}$: the wave transport velocity

$\dfrac{1}{h} (\partial_z B_y)$: the vector potential transport velocity.

$\dfrac{\langle \eta_0 u_0 \rangle}{h} - \dfrac{1}{h} (\partial_z B_y)$: the Stokes drift.

w : vertical velocity in the stretched vertical coordinate

w_0 : $w - \langle w \rangle$ short-term or high pass filtered component of w

$\langle w_1 \rangle$: long-term or low pass filtered component of w

H : total depth of the water column

h : still water depth

u_1 : horizontal mass transport (or Lagrangian mean) velocity

w_1 : vertical mass transport (or Lagrangian mean) velocity

B_y : vector potential

K_v : vertical turbulent diffusion coefficients

In a stretched vertical coordinate, the Eulerian residual and wave transport velocity are combined to form Eulerian residual transport velocity which satisfies the continuity equation.

$$u_{er} = \langle u_1 \rangle + \dfrac{\langle \eta_0 u_0 \rangle}{h}$$

The operator $\langle \ \rangle$ could be defined as a low pass filter with an ideal representation in the frequency domain of

$$L = \{ \begin{matrix} 1 \\ 0 \end{matrix} \qquad \begin{matrix} 0 <= \omega <= \omega_1 \\ \omega_1 <= \omega <= \infty \end{matrix} \qquad (5.2.5)$$

where $\omega_1 <= (\omega_0 \omega_2)$, with $\omega_2 = F^2 \omega_0$. Assuming tidal forcing consists of N_2 and M_2 tide, the calculation of $\langle \eta_0 u_0 \rangle$ is carried out as follows:

Let $\omega_1 = \omega_{M_2} - \omega_{N_2}$ $\qquad \omega_1$: modulation component

$\omega_2 = \omega_{N_2}$, $\omega_3 = \omega_{M_2}$ $\qquad \omega_2$ and ω_3 tide forcing components.

$\omega_4 = 2\omega_{N_2}$, $\omega_5 = 2\omega_{N_2}$ $\qquad \omega_4$ and ω_5 harmonics of forcing.

Let $u_0^{N_2} = a_2^u \cos(\omega_2 t) + b_2^u \sin(\omega_2 t)$ $\qquad N_2$ component of $u_{i,k}$

$u_0^{M_2} = a_3^u \cos(\omega_3 t) + b_3^u \sin(\omega_3 t)$ $\qquad M_2$ component of $u_{i,k}$.

$u_1^{M_2 - N_2} = a_1^u \cos(\omega_1 t) + b_1^u \sin(\omega_1 t)$ $\qquad$ Modulation of $u_{i,k}$.

$w_0^{N_2} = a_2^w \cos(\omega_2 t) + b_2^w \sin(\omega_2 t)$ $\qquad N_2$ component of $w_{i,k}$.

$w_0^{M_2} = a_3^w \cos(\omega_3 t) + b_3^w \sin(\omega_3 t)$ $\qquad M_2$ component of $w_{i,k}$.

$w_1^{M_2 - N_2} = a_1^w \cos(\omega_1 t) + b_1^w \sin(\omega_1 t)$ $\qquad$ Modulation of $w_{i,k}$.

$\eta_0^{N_2} = a_2^\eta \cos(\omega_2 t) + b_2^\eta \sin(\omega_2 t)$ $\qquad N_2$ component of η_i.

$$\eta_0^{M_2} = a_3^{\eta}\cos(\omega_3 t) + b_3^{\eta}\sin(\omega_3 t) \qquad M_2 \text{ component of } \eta_i.$$

$$\eta_1^{M_2-N_2} = a_1^{\eta}\cos(\omega_1 t) + b_1^{\eta}\sin(\omega_1 t) \qquad \text{Modulation of } \eta_i.$$

Modulation of $\eta_0 u_0$ is obtained by the low pass filter as follows:

$$\langle \eta_0 u_0 \rangle = \langle (\eta_0^{N_2} + \eta_0^{M_2})(u_0^{N_2} + u_0^{M_2}) \rangle \qquad (5.2.6)$$

$$= \langle h_0^{N_2} u_0^{N_2} + \eta_0^{M_2} u_0^{M_2} + \eta_0^{N_2} u_0^{M_2} + \eta_0^{M_2} u_0^{N_2} \rangle$$

$$= \frac{1}{2}\{ [a_2^u a_2^{\eta} + b_2^u b_2^{\eta}] + [a_3^u a_3^{\eta} + b_3^u b_3^{\eta}]\}$$

$$+ \frac{1}{2}\{ (a_3^u a_2^{\eta} + b_3^u b_2^{\eta})\cos(\omega_1 t) + (b_3^u a_2^{\eta} - a_3^u b_2^{\eta})\sin(\omega_1 t) \}$$

$$+ \frac{1}{2}\{ (a_2^u a_3^{\eta} + b_2^u b_3^{\eta})\cos(\omega_1 t) + (a_2^u b_3^{\eta} - b_2^u a_3^{\eta})\sin(\omega_1 t) \}$$

define $\bar{A}$ as the time average of variable A or steady component of A, the following is obtained:

$$\langle u_1 \rangle = \bar{u} + a_1^u \cos\omega_1 t + b_1^u \sin\omega_1 t \qquad (5.2.7)$$

$$\langle w_1 \rangle = \bar{w} + a_1^w \cos\omega_1 t + b_1^w \sin\omega_1 t \qquad (5.2.8)$$

$$\langle K_{v1} \rangle = \bar{K}_v + a_1^{Kv} \cos\omega_1 t + b_1^{Kv} \sin\omega_1 t \qquad (5.2.9)$$

The potential B_y is obtained as follows:

$$B_y = \langle\, w_0 \int u_0\, dt\, \rangle \tag{5.2.10}$$

$$= \langle\, \{\, a_2^W\cos(\omega_2 t) + b_2^W\sin(\omega_2 t) + a_3^W\cos(\omega_3 t) + b_3^W\sin(\omega_3 t)\, \}*$$

$$\int\{\, a_2^u\cos(\omega_2 t) + b_2^u\sin(\omega_2 t) + a_3^u\cos(\omega_3 t) + b_3^u\sin(\omega_3 t)\, \}dt$$

$$\rangle$$
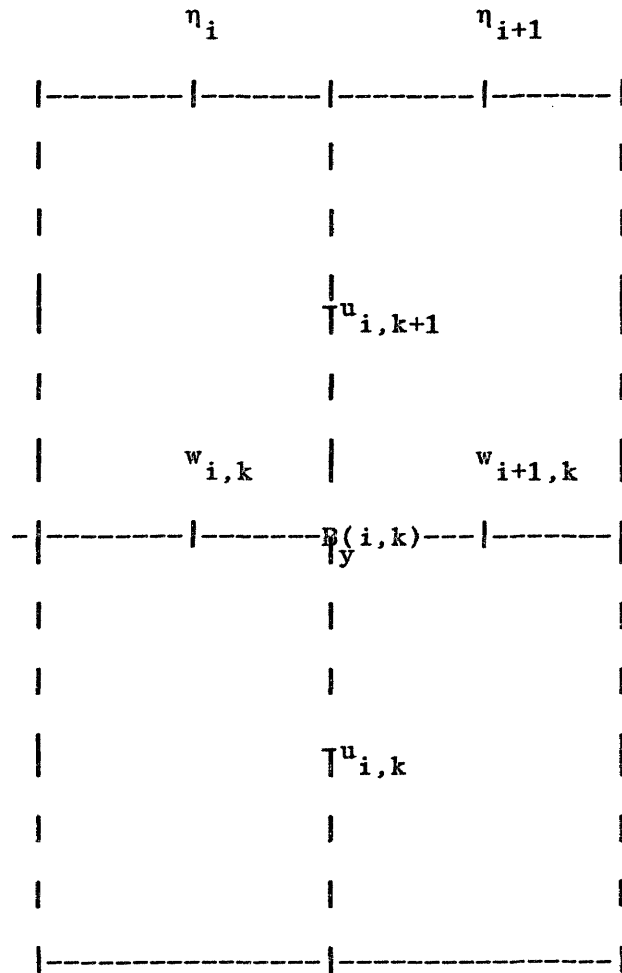
after algebraic simplifications, the final B_y is as follows:

$$B_y = -\frac{1}{2}\{\frac{b_3^W a_3^u}{\omega_3} - \frac{a_3^W b_3^u}{\omega_3} + \frac{b_2^W a_2^u}{\omega_2} - \frac{a_2^W b_2^u}{\omega_2}\} \tag{5.2.11}$$

$$+\frac{1}{2}\{\frac{a_2^W a_3^u}{\omega_3} + \frac{b_2^W b_3^u}{\omega_3} - \frac{a_3^u a_2^u}{\omega_2} - \frac{b_3^W b_2^u}{\omega_2}\}\sin(\omega_1 t)$$

$$+\frac{1}{2}\{\frac{b_2^W a_3^u}{\omega_3} - \frac{a_2^W b_3^u}{\omega_3} + \frac{b_3^W a_2^u}{\omega_2} - \frac{a_3^W b_2^u}{\omega_2}\}\cos(\omega_1 t)$$

Note, all the index i, k for harmonic coefficients are omitted for clarity and convenience.

From the expressions above, the lowest order approximation to the Lagrangian residual velocity $u_1(i,k)$ and $w_1(i,k)$ could be obtained by substituting corresponding harmonic coefficients averaged at the given point into the expressions for them according to the following diagram and the discrete expressions:

```
         η
          i                    η
                                i+1
|--------|-------|--------|-------|
|        |                |       |
|        |                |       |
|        |                |       |
|        |       |  u      |       |
|        |       T  i,k+1  |       |
|        |                |       |
|   w    |                |   w    |
|    i,k |                |    i+1,k|
-|--------|-------B (i,k)---|-------|
|        |       T y       |       |
|        |                |       |
|        |                |       |
|        |   u             |       |
|        T    i,k          |       |
|        |                |       |
|        |                |       |
|--------------|----------------|
```

$$u_1(i,k) = \langle\, u_1(i,k)\, \rangle$$

$$+ \frac{\langle \eta_0^*(i)u_0(i,k)\rangle}{h} - \frac{1}{h}\left(\frac{B_y(i,k)-B_y(i,k-1)}{\Delta z}\right) \qquad (5.2.12)$$

where $\eta_0^* = 0.5 * (\eta_0(i) + \eta_0(i+1))$

$$w_1(i,k) = \langle\, w_1(i,k)\, \rangle + \left(\frac{B_y(i,k)-B_y(i-1,k)}{\Delta x}\right) \qquad (5.2.13)$$

6. Numerical Experiment

6.1   Introduction

To start the numerical model, one must first set up suitable initial conditions, i.e., setting all the velocity variables and the surface elevation to zero, setting the initial salinity field, and then imposing a spring-neap tide forcing at the mouth as the boundary condition. And let time advance one step, after renewed surface elevations and velocities are obtained, they will be substituted into the salinity transport equation to get the renewed salinity field. The renewed salinity values are then substituted back into the momentum equation in the density forcing terms to get a new velocity field. These calculations are repeated until an equilibrium state is reached. At that time the harmonic least squares filter is activated to calculate the filtered residual current. All the residual variables, such as the Eulerian, Lagrangian, wave transport and vector potential transport velocities can be obtained at the end of the model run according to the algorithm presented in Chapter 5.

6.2   Test Run of The Numerical Model

To facilitate the interpretation of the output data from the numerical model, the dimensional form of the equations is used in the numerical simulation. The number of vertical layers is set to 10 and the number of horizontal grid intervals is set to 20. To observe the

effect and mechanism of spring-neap tide forcing on the mixing processes in an estuary, a channel of length 150 km with a constant depth of 10 meters is assumed, i.e. Δx is set to 7500 meter and h to 10 meter. The time step selected is 1118.0 seconds, which is about 18 minutes. A much longer time step (e.g. 36 minutes) could be used but then accuracy might be a problem. The fresh water discharge is set to 0.0075 m/sec, which corresponds to 75 m^3/sec if a channel width of 1000 m is assumed. The roughness height z_0 equals 0.002m, and the drag coefficient C_D is 0.004. The modulated tidal forcing is a combination of N2 and M2 tides amplitudes equal to 0.36 meter and 0.18 meter respectively (Figure 6.1). With these data, the model ran first for 3000 steps (about 60 M2 tide cycles) to let the transients die out and then the simulation of the estuary circulation with spring-neap tide forcing continues for another 32 days with the least squares harmonic filter turned on in the mean while.

Figure 6.1   Spring-Neap tide Forcing at the Mouth of Channel

with M2 = 0.36 m, N2 = 0.18 m.
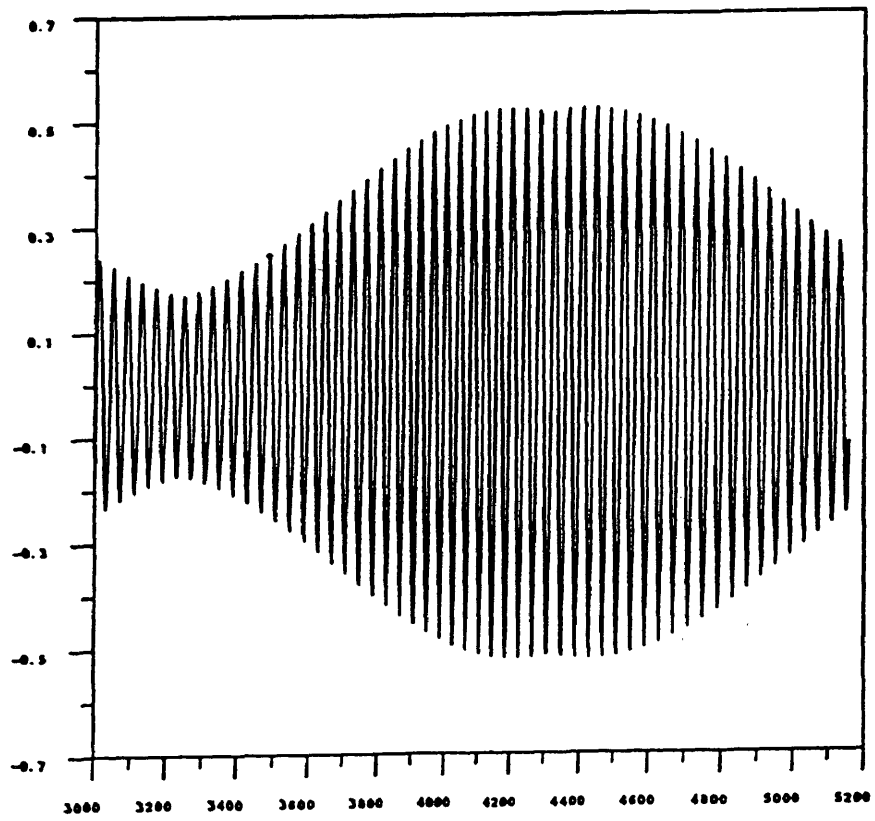
6.3 Empirical Parameters for the Algebraic Turbulence Model

The empirical constants for turbulence model A_1, B_1, A_2, B_2, C_1 can be obtained from neutral density turbulent flow experiments. In the numerical simulation, the parameter values used are as follows (Mellor and Yamada, 1982):

$$(A_1, B_1, A_2, B_2, C_1) = (0.92, 16.6, 0.59, 10.1, 0.08)$$

while the Prandtl constant P_r^N is set equal to 1. The corresponding model stability function parameters $(R_{fc}, R_{f1}, R_{f2}, R_{ic})$ are $(0.191, 0.245, 0.223, 0.293)$. These values are rounded off further to make them look more elegant and reflect the average value of the experiments.

$$R_{fc} = 1/6$$

$$R_{f1} = 1/4$$

$$R_{f2} = 1/5, \qquad P_R^N = 1 \text{ which gives}$$

$$R_{ic} = 1/3 \ ,$$

The above values are used in the test run of the numerical model.

6.4   Presentation of the Results

6.4.1   Residual Salinity

The output residual salinity fields along the channel were plotted as contour plots at 4 day interval during the spring-neap tide forcing for 32 days, the time intervals are 4 days before neap tide, neap tide, 4 days after neap tide, 8 days after neap tide, 12 days after neap tide, 2 days after spring tide, 6 days after spring tide, and 10 days after spring tide which is the repetition of 4 days before the neap tide (Figure-6.2, 6.3, 6.4, 6.5). Examining the plots, the modulation of the stratification in the middle of the channel is clearly shown. Starting from Figure-6.3 to Figure-6.5, the hypothetical estuary gradually experiences stratification, and then de-stratification and then stratification again with the spring-neap tide forcing. The strongest stratification occurs during the neap tide (Figure-6.2), while during the period between 12 days after the neap and 2 days after the spring tide (Figure-6.4), the channel is destratified except near the head of the channel where fresh water comes in, there is a slight stratification.

Figure 6.2   Contour Plot of Modulated Salinity with

Spring-Neap Tide Forcing

Contour Plot of Salinity With Spring-Neap Tide Forcing
(M2=0.36M, N2=0.18M, Q=$-0.07M^2Sec^{-1}$, CB=0.004, DT=1118. Sec)
4 Days Before Neap Tide

Neap Tide

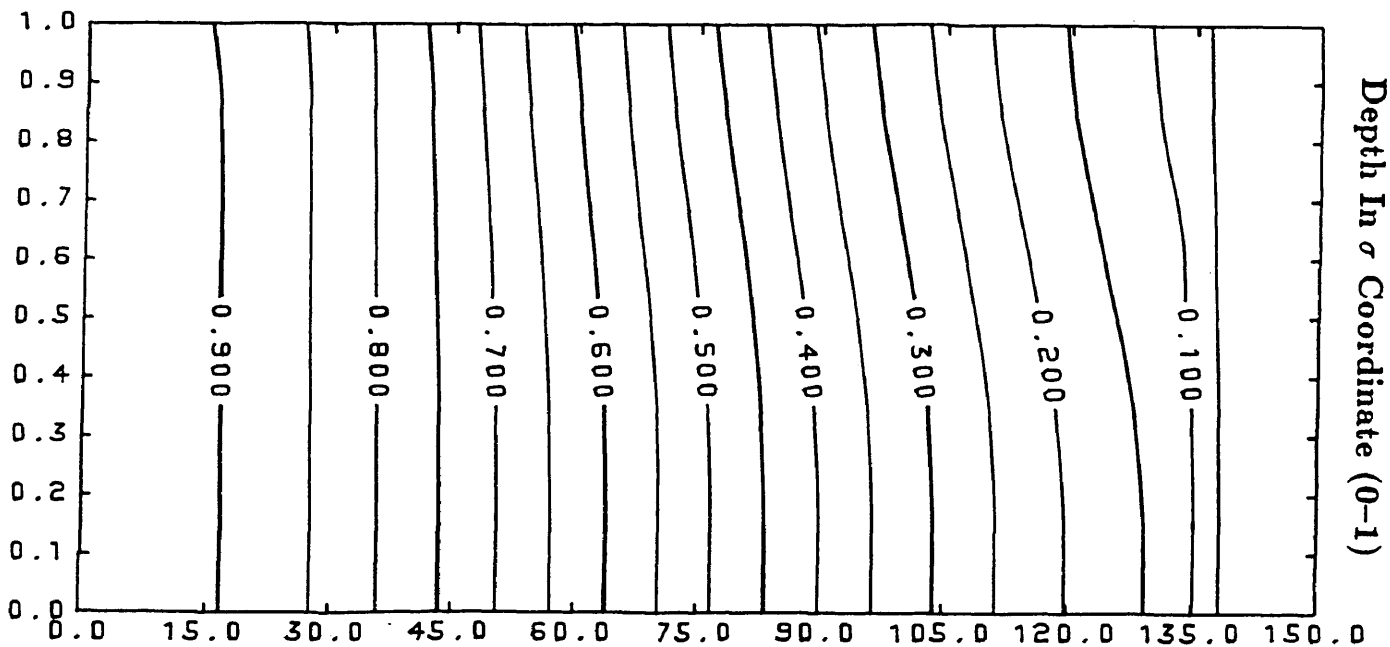Channel Length 150 Km

Depth In σ Coordinate (0-1)
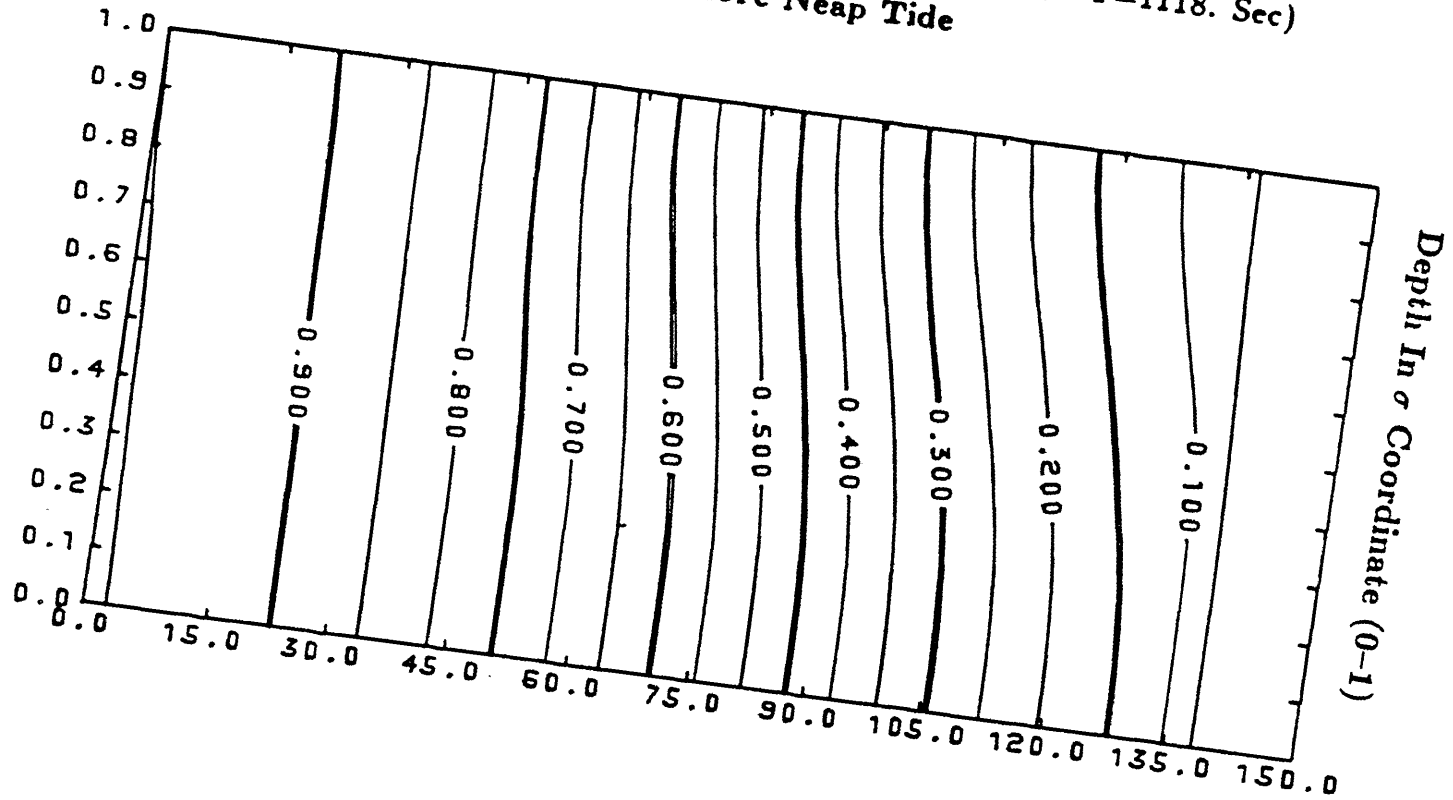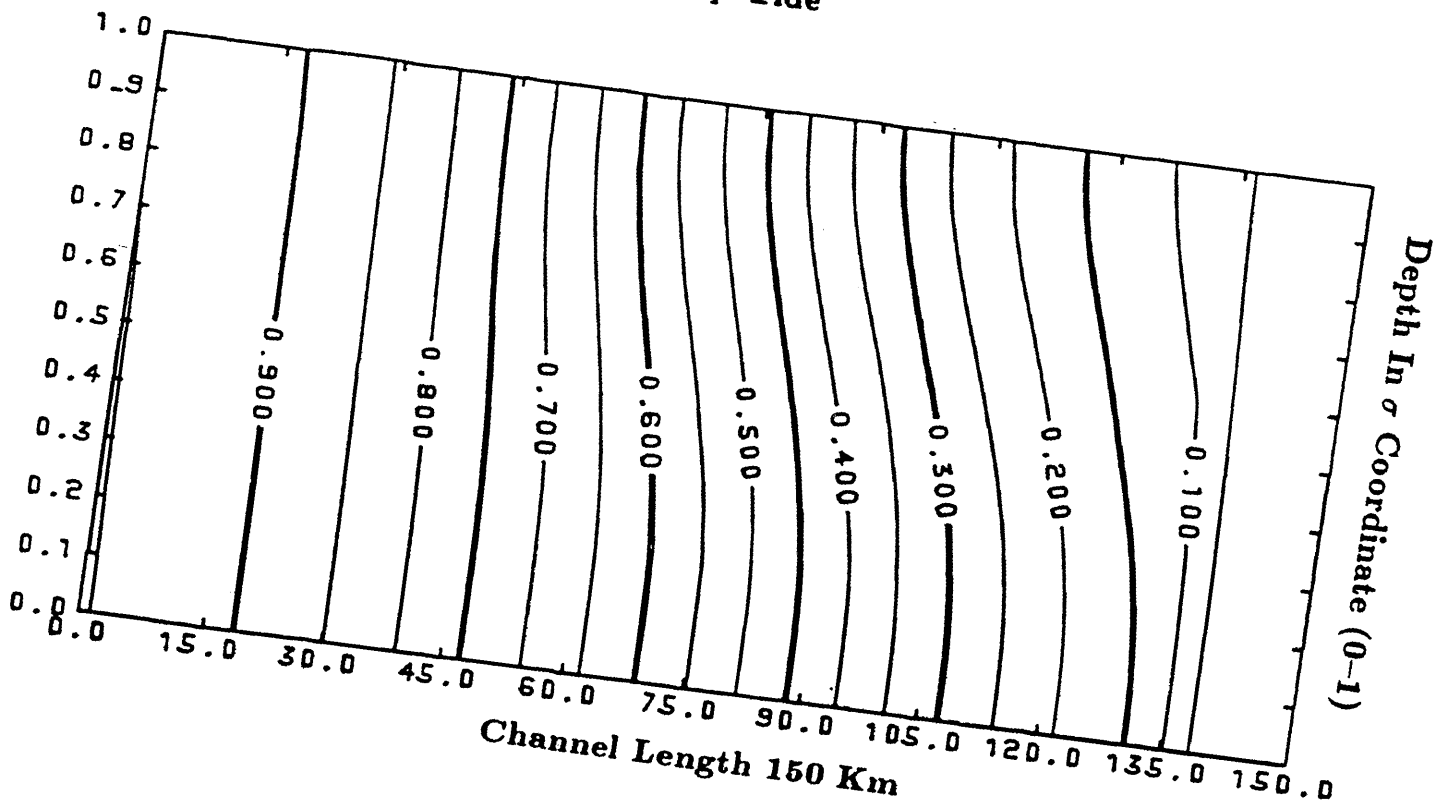
Figure 6.3   Contour Plot of Modulated Salinity with

Spring-Neap Tide Forcing
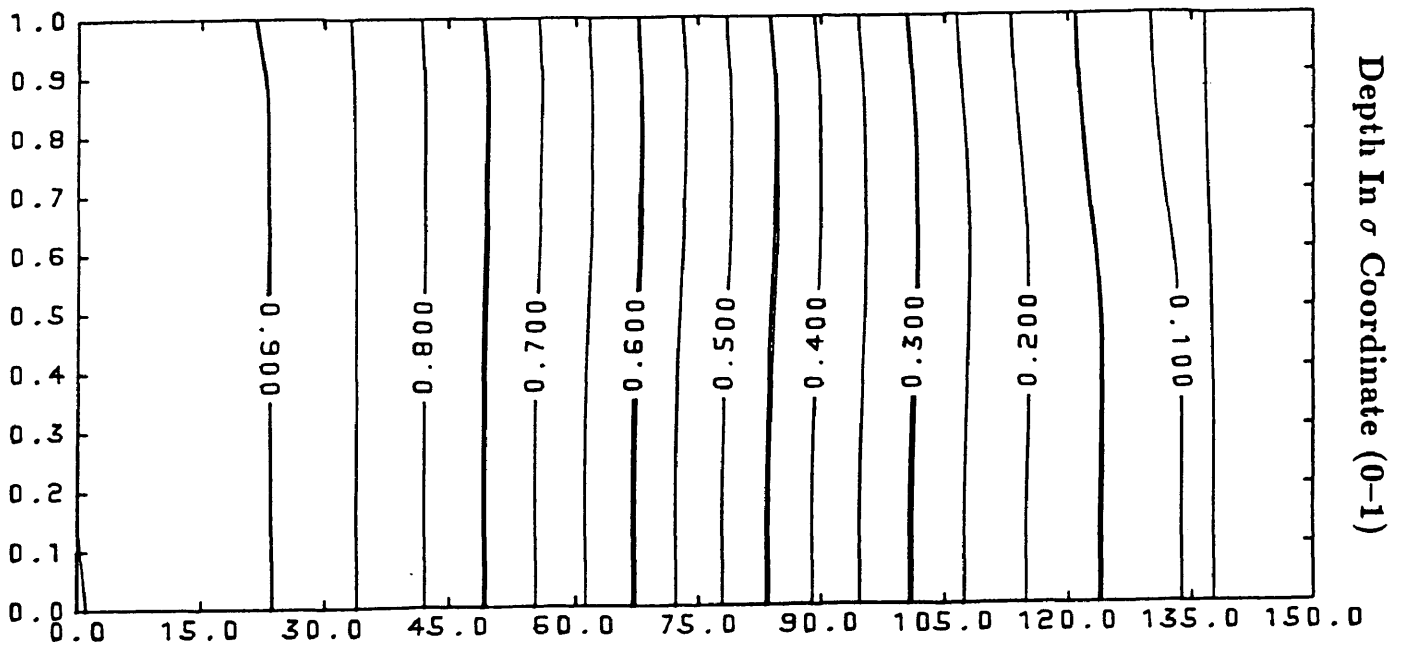
4 Days After Neap Tide
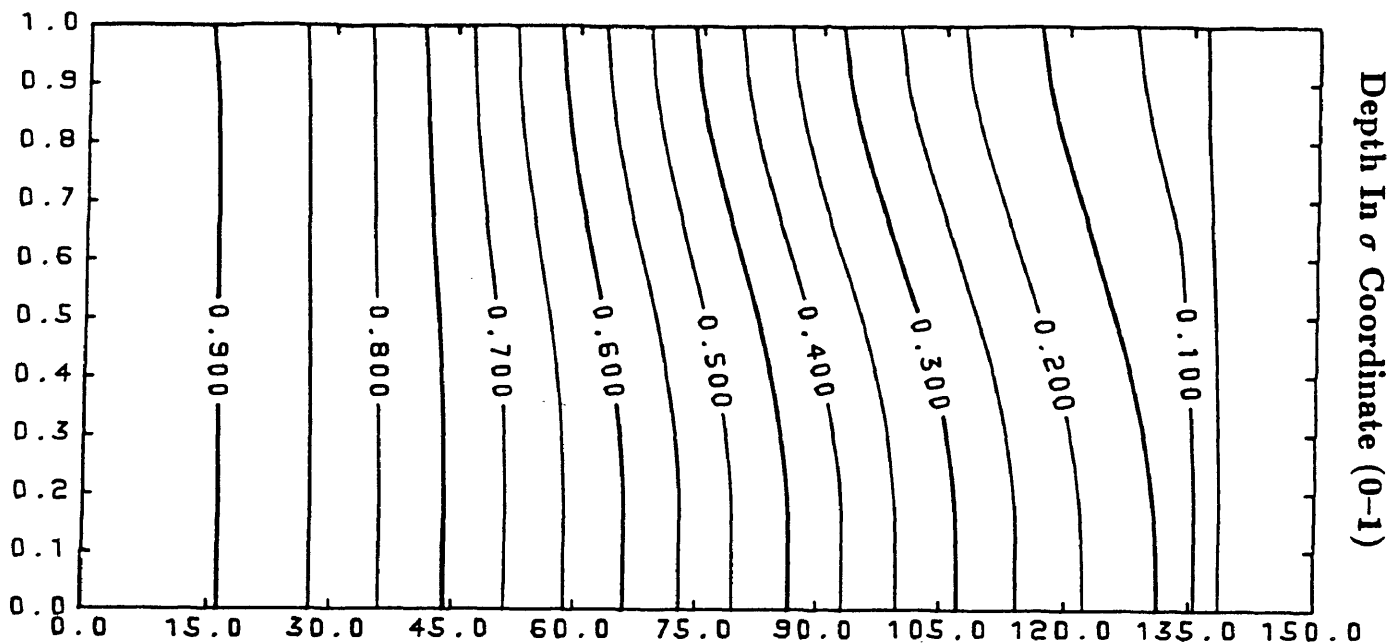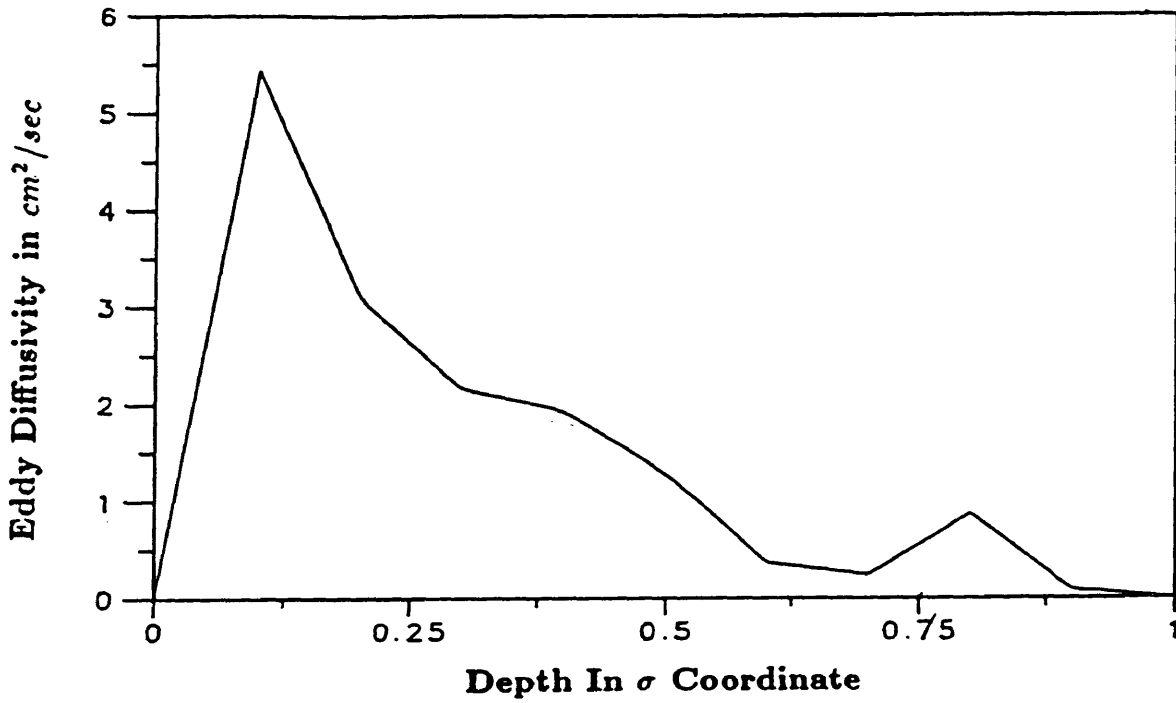

8 Days After Neap Tide

Channel Length 150 Km

Figure 6.4   Contour Plot of Modulated Salinity with

Spring-Neap Tide Forcing

12 Days After Neap Tide

Depth In σ Coordinate (0-1)

0.900 0.800 0.700 0.600 0.500 0.400 0.300 0.200 0.100

2 Days After Spring Tide

Depth In σ Coordinate (0-1)

0.900 0.800 0.700 0.600 0.500 0.400 0.300 0.200 0.100
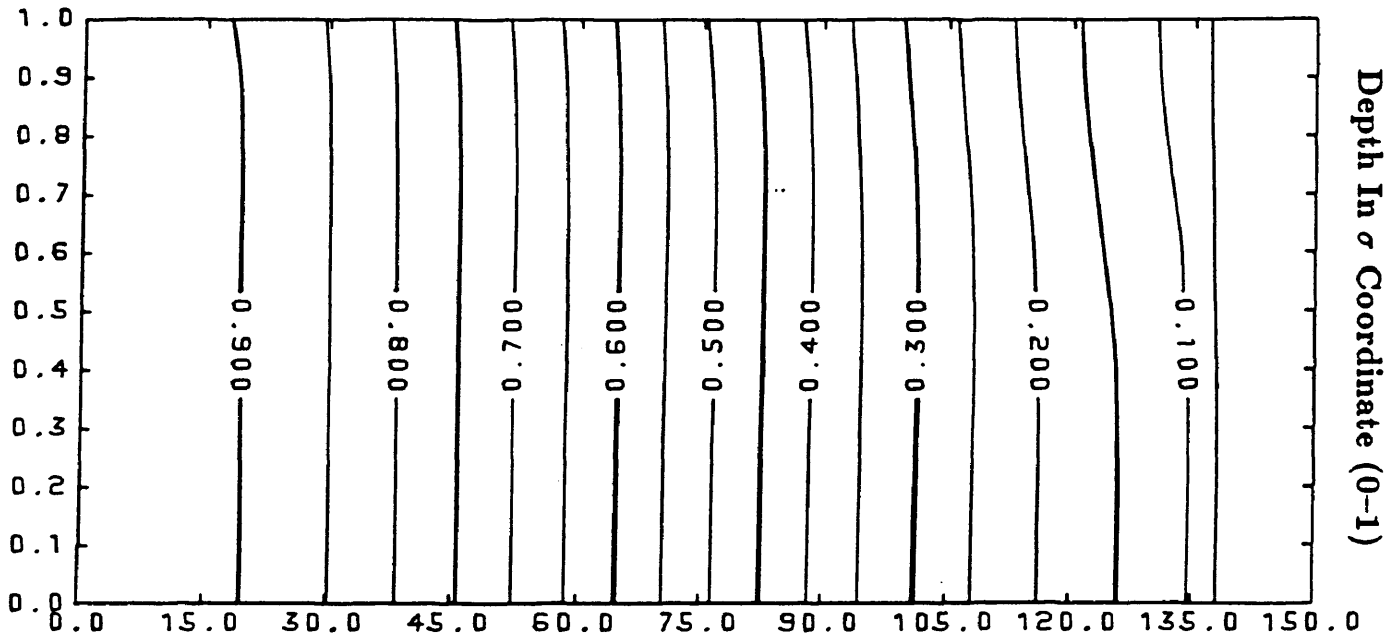
Channel Length 150 Km

Figure 6.5   Contour Plot of Modulated Salinity with

Spring-Neap Tide Forcing

6 Days After Spring Tide

10 Days After Spring Tide

Channel Length 150 Km

6.4.2　Residual Vertical Mixing

The mid-channel section was examined for the residual vertical turbulent mixing coefficients or eddy diffusivity (Figure-6.6, 6.7, 6.8, 6.9), also at the time interval of 4 days during the spring-neap tide forcing for 32 days. From Figure 6.6 to Figure 6.9, the vertical profile of the eddy diffusivity coefficient show changes with the spring-neap tide. During the neap tide, the vertical profiles of the eddy diffusivity show a valley with two peaks. This clearly indicates the stratification of the channel because saltier water is not able to mix upward easily with fresher surface water. It is also worth noting that the position of the valley of the profile moves with the changing amplitude of the tide forcing. At 4 days before or after neap tide, the valley is located at the depth of corresponding to 75 per cent of the total depth, while at neap tide, the valley moves to the mid-depth. At the neap tide, the valley drops to its lowest point or minimum value (0.1 cm^2/sec. note: the vertical scale here is not the same for each plot). After neap tide, the eddy diffusivity values gradually increase because of stronger turbulence mixing, During the period between 12 days after the neap tide and 2 days before the spring tide, the valley disappears and the average eddy viscosity reaches about 5 cm^2/sec. ,which is an indication of good vertical mixing of the saltier bottom water and the fresher surface water. This is consistent with the modulated salinity distribution in Figure-6.2 to Figure 6.5.

79

Figure 6.6   Modulated Mid-Channel Eddy Diffusivity Profile

with Spring-Neap Tide Forcing

Modulatd Mid-Channel Eddy Diffusivity With Spring-Neap Tide Forcing
$$(M2 = 0.36M, N2 = 0.18M, Q = -0.075M^2 Sec^{-1}, L_c = 150 Km)$$
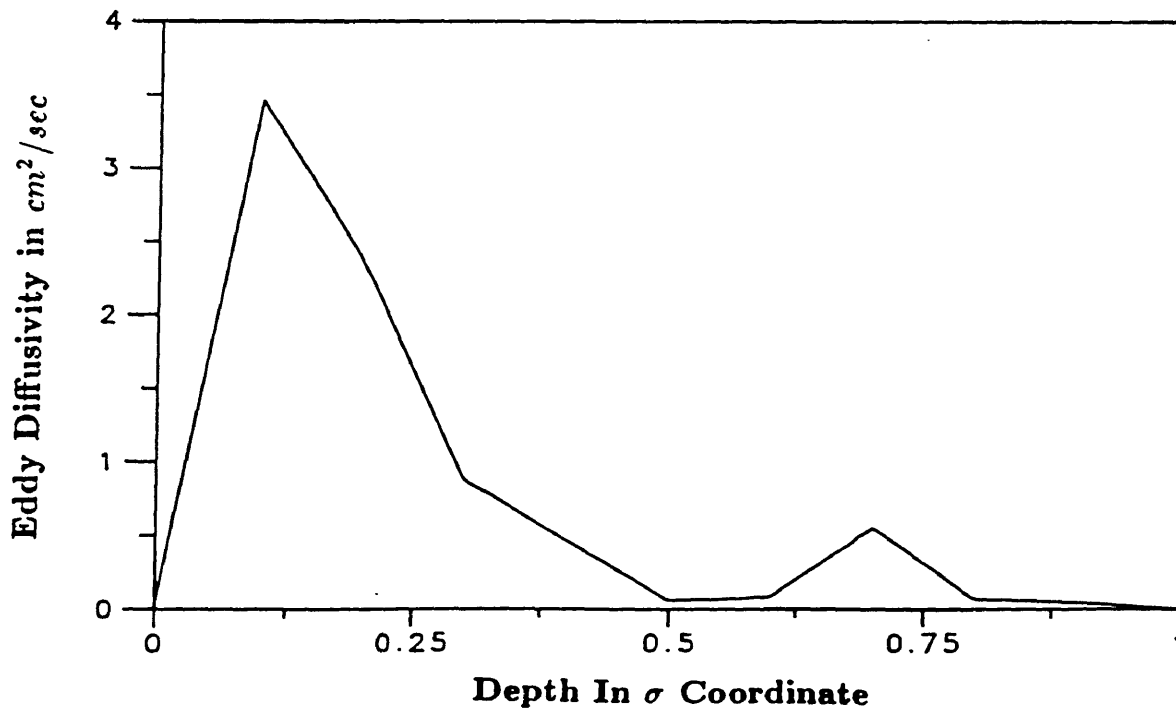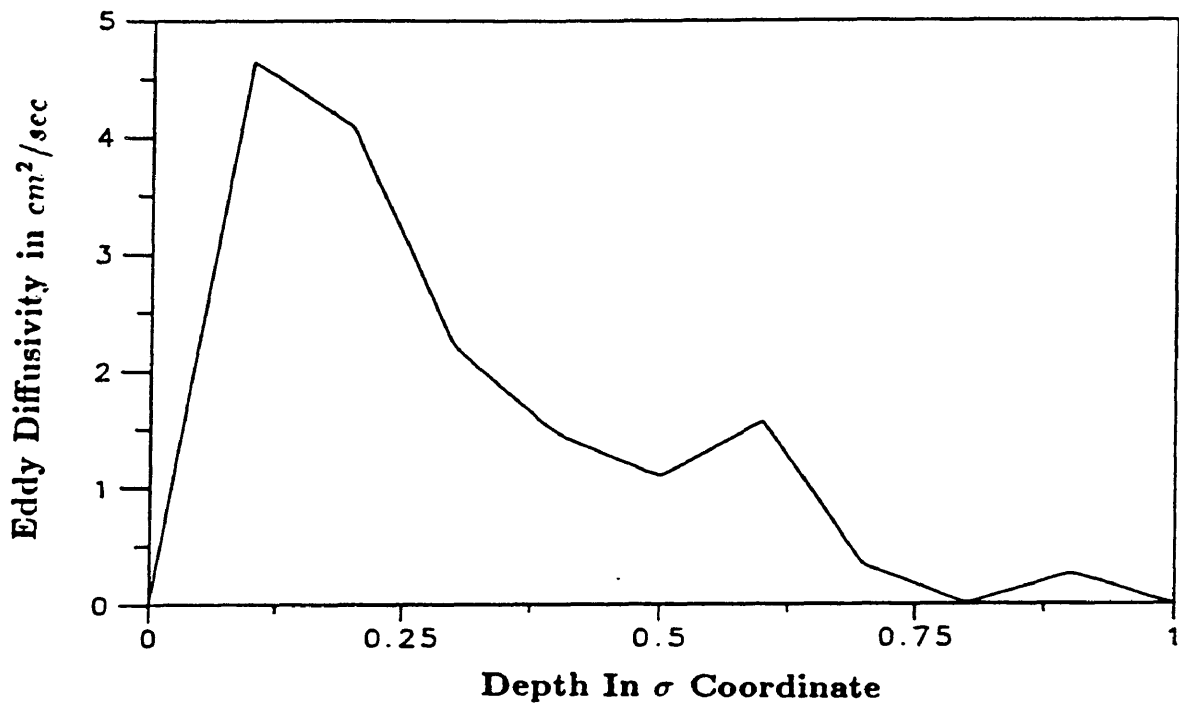### 4 Days Before Neap Tide

Eddy Diffusivity in cm^2/sec

Depth In σ Coordinate

Neap Tide

Eddy Diffusivity in cm^2/sec

Depth In σ Coordinate

Figure 6.7   Modulated Mid-Channel Eddy Diffusivity Profile

with Spring-Neap Tide Forcing

4 Days After Neap Tide

Eddy Diffusivity in cm^2/sec

Depth In σ Coordinate

8 Days After Neap Tide

Eddy Diffusivity in cm^2/sec

Depth In σ Coordinate
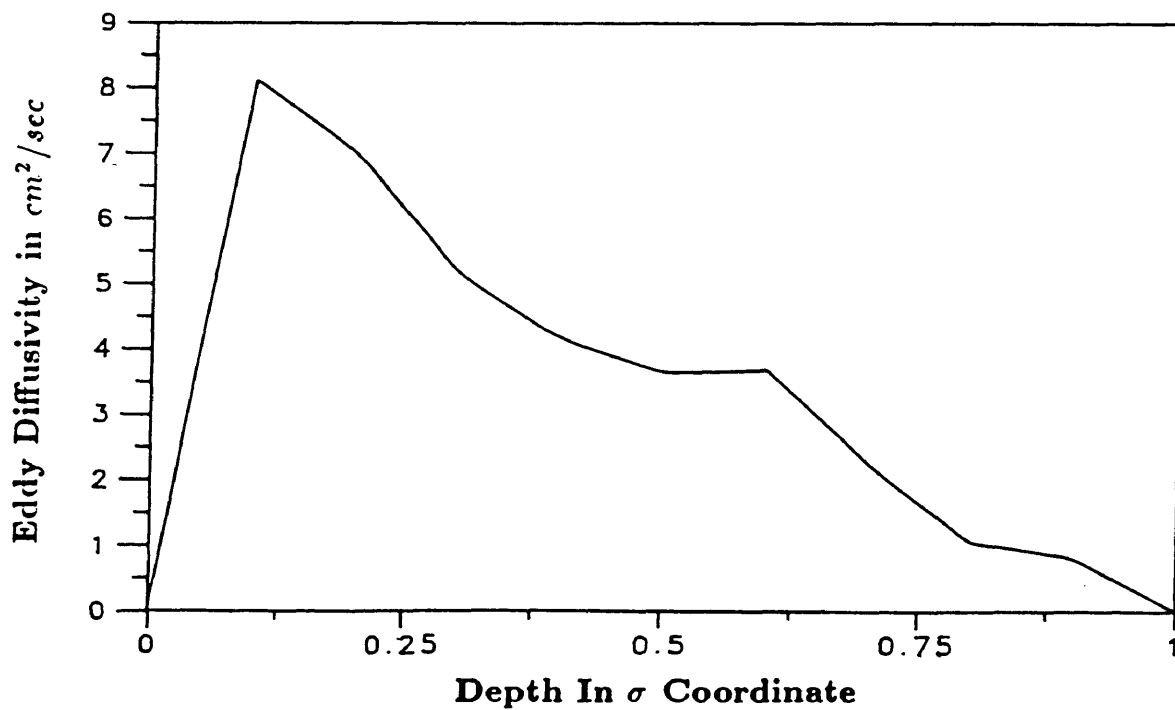
Figure 6.8 Modulated Mid-Channel Eddy Diffusivity Profile

with Spring-Neap Tide Forcing
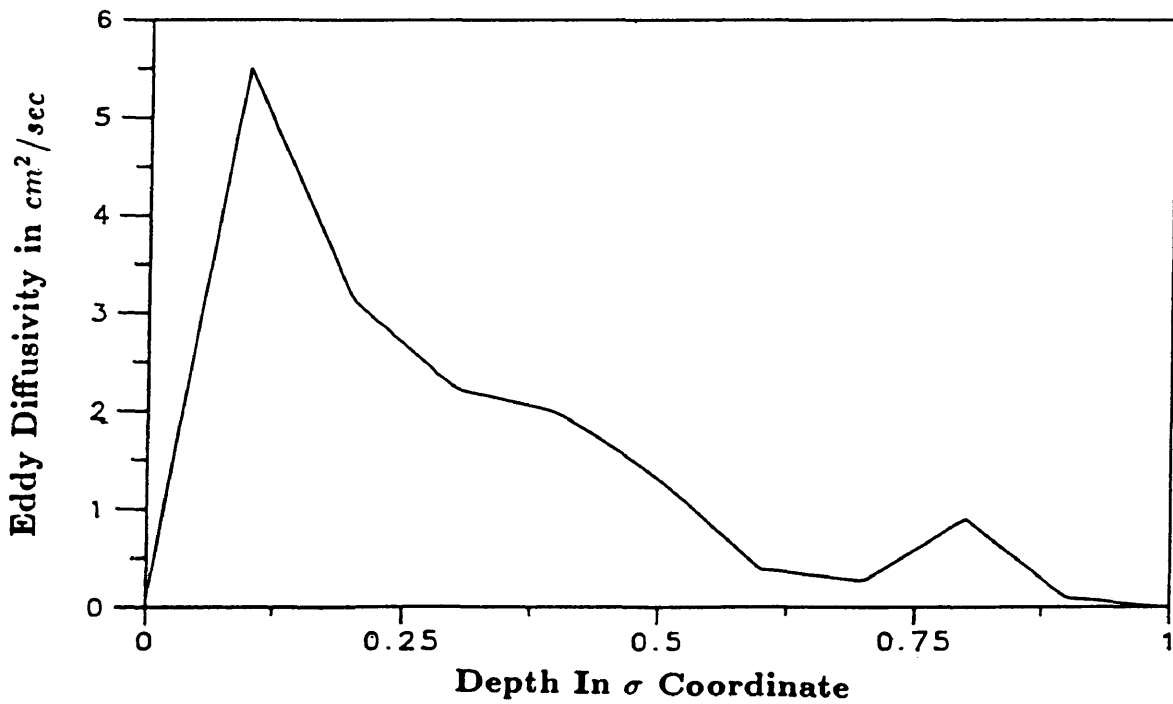
12 Days After Neap Tide
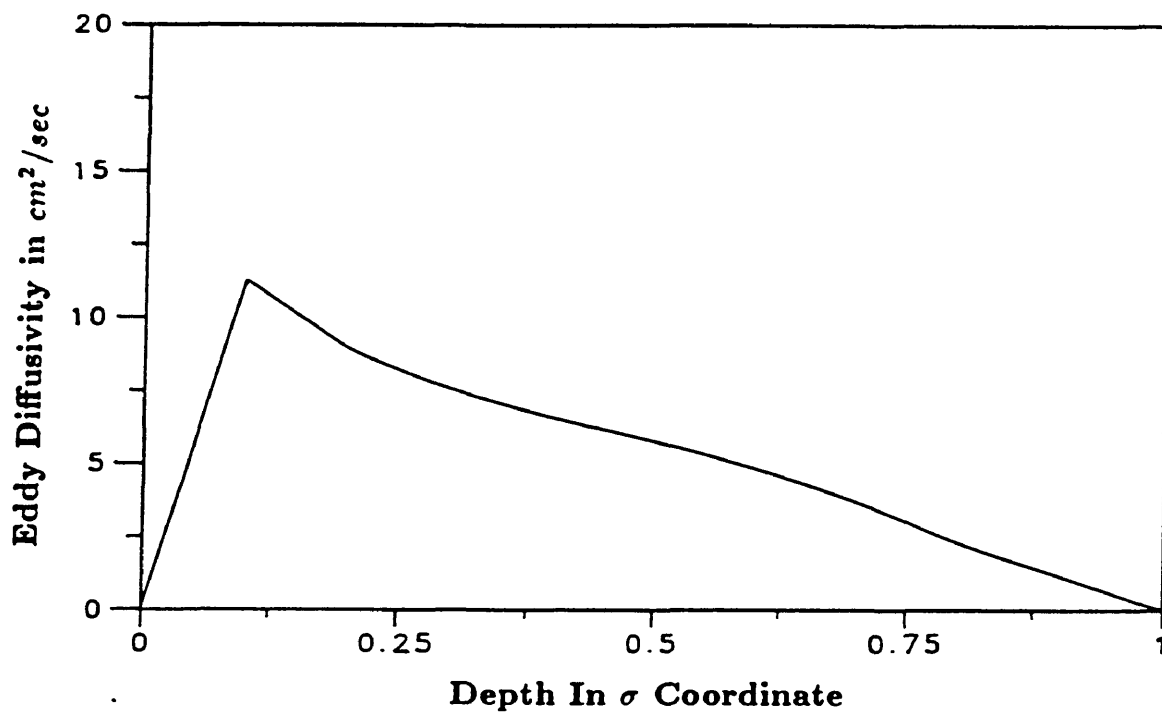
2 Days After Spring Tide
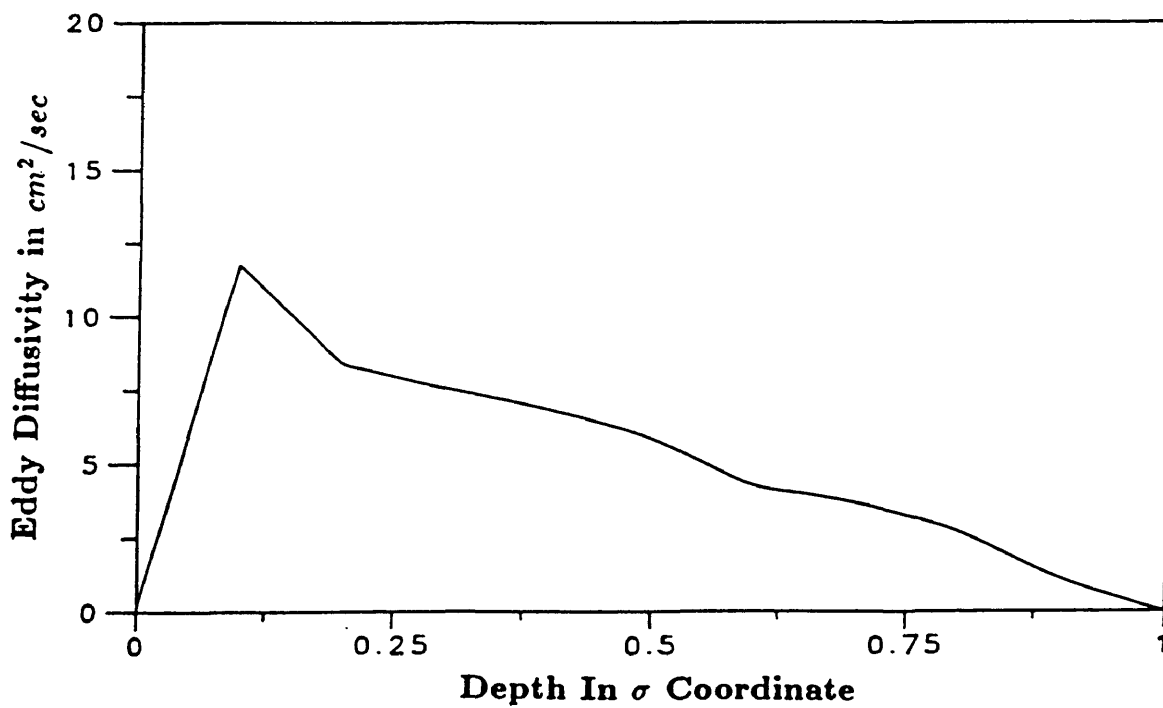
Figure 6.9   Modulated Mid-Channel Eddy Diffusivity Profile

with Spring-Neap Tide Forcing

6 Days After Spring Tide
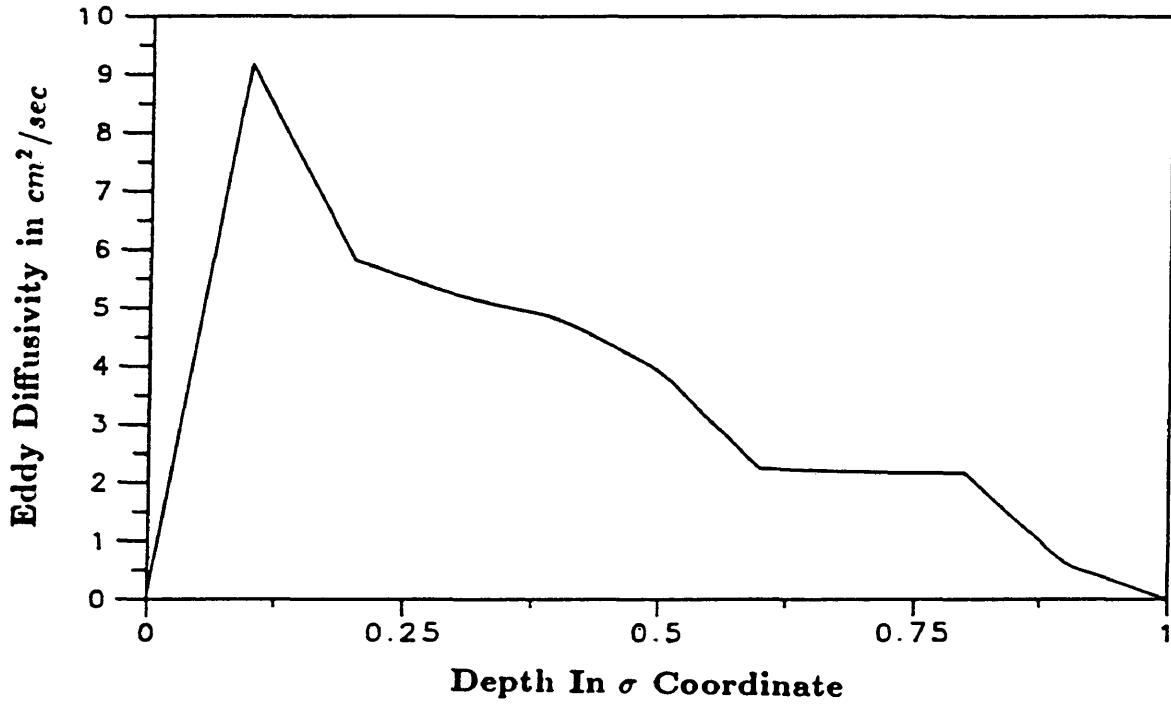

10 Days After Spring Tide

6.4.3 Lagrangian Residual Velocity

To visualize the modulation of the Lagrangian residual velocity, the velocity outputs from the numerical simulation is plotted in the form of a vector plot as shown in Figure 6.10 to Figure 6.13. The time interval of each plot is the same, 4 days interval for each plot, for 32 days during the spring–neap tide forcing. The Lagrangian velocity vector plot clearly shows the residual two–layer circulation with the upper surface fresher water flowing seaward and the bottom saltier water flowing landward. The strength of this two–layer circulation is also modulated by the spring–neap forcing as can be seen from the Figures 6.10 to Figure 6.13. For the mid–channel section, the strongest two–layer circulation occurs during neap tide when the hypothetical estuary is stratified and the weakest two–layer circulation occurs during spring tide when the estuary is destratified.

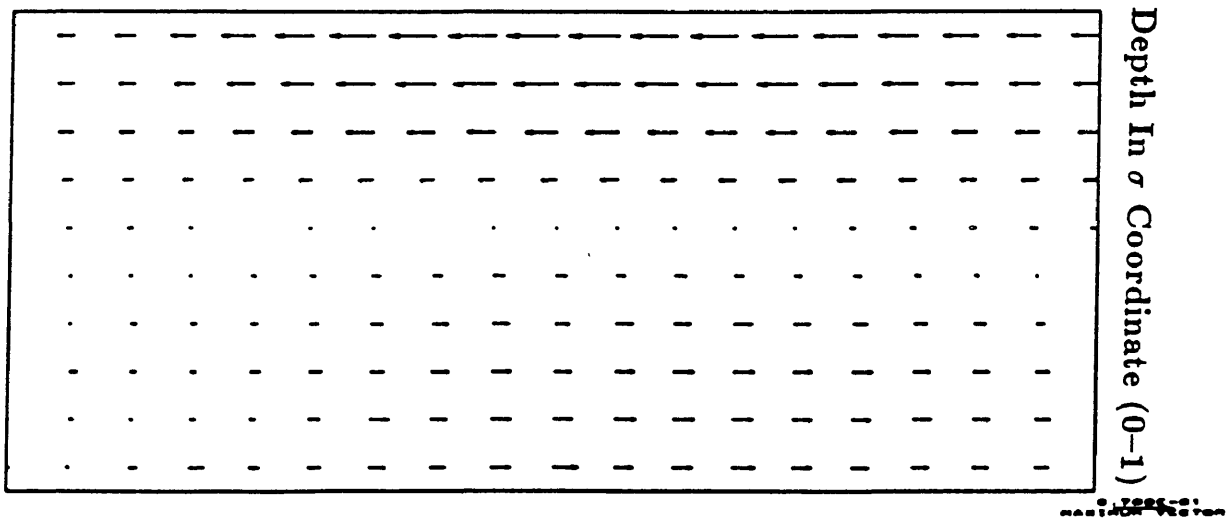Figure 6.10   Modulated Lagrangian Residual Velocity with

Spring—Neap Tide Forcing

Lagrangian Residual With Spring-Neap Tide Forcing
($M2 = 0.36M, N2 = 0.18M, Q = -0.07M^2Sec^{-1}, L_c = 150Km$)
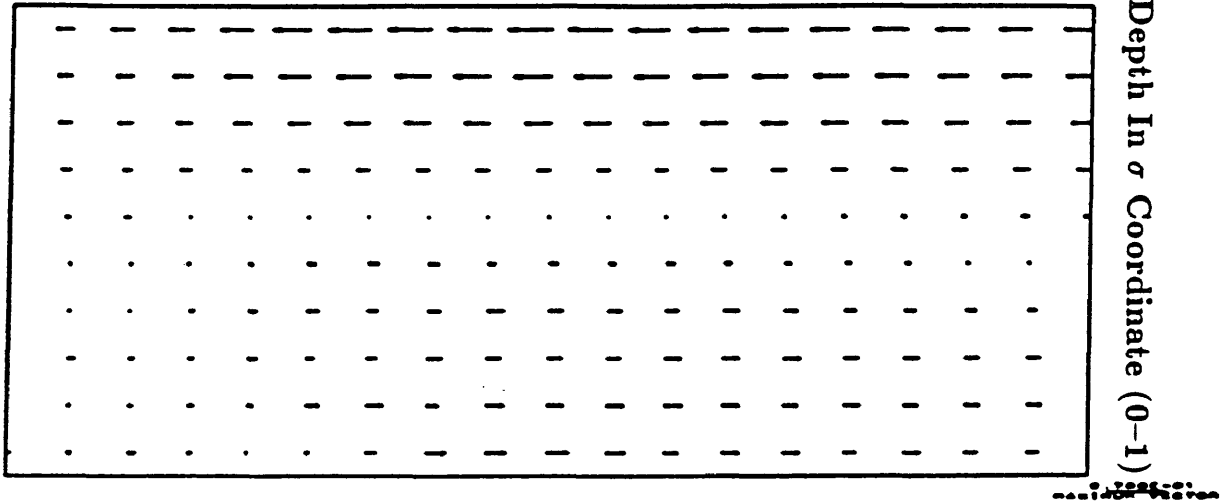
4 Days Before Neap Tide
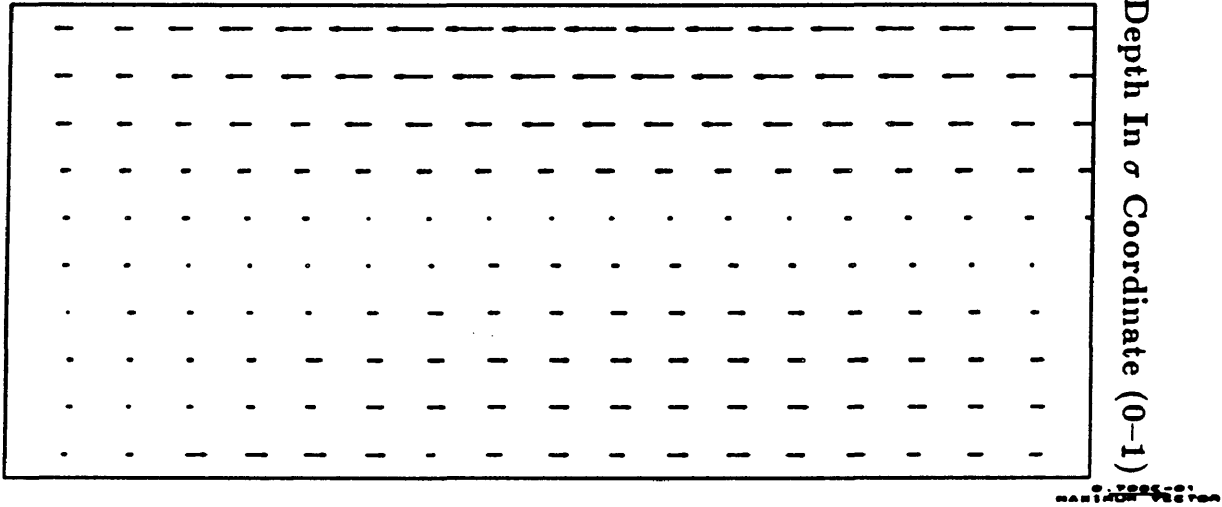
Channel Length 150 Km

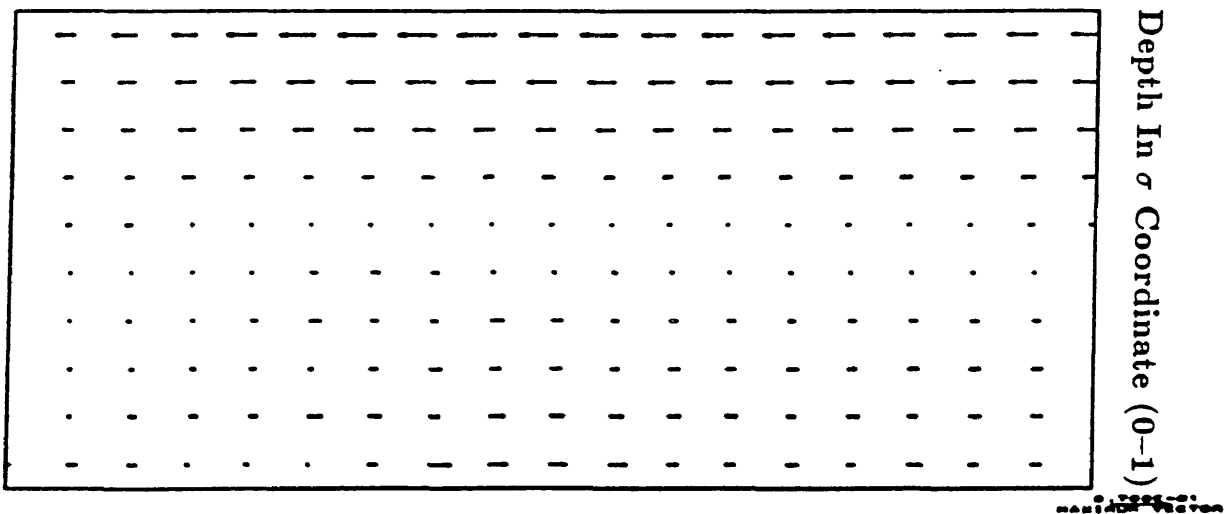## Neap Tide

Channel Length 150 Km

Figure 6.11   Modulated Lagrangian Residual Velocity with

Spring-Neap Tide Forcing

4 Days After Neap Tide

Depth In σ Coordinate (0-1)

Channel Length 150 Km

8 Days After Neap Tide

Depth In σ Coordinate (0-1)

Channel Length 150 Km

Figure 6.12   Modulated Lagrangian Residual Velocity with

Spring-Neap Tide Forcing

12 Days After Neap Tide

Depth In σ Coordinate (0-1)

Channel Length 150 Km

2 Days After Spring Tide

Depth In σ Coordinate (0-1)

Channel Length 150 Km

Figure 6.13   Modulated Lagrangian Residual Velocity with

Spring-Neap Tide Forcing

6 Days After Spring Tide
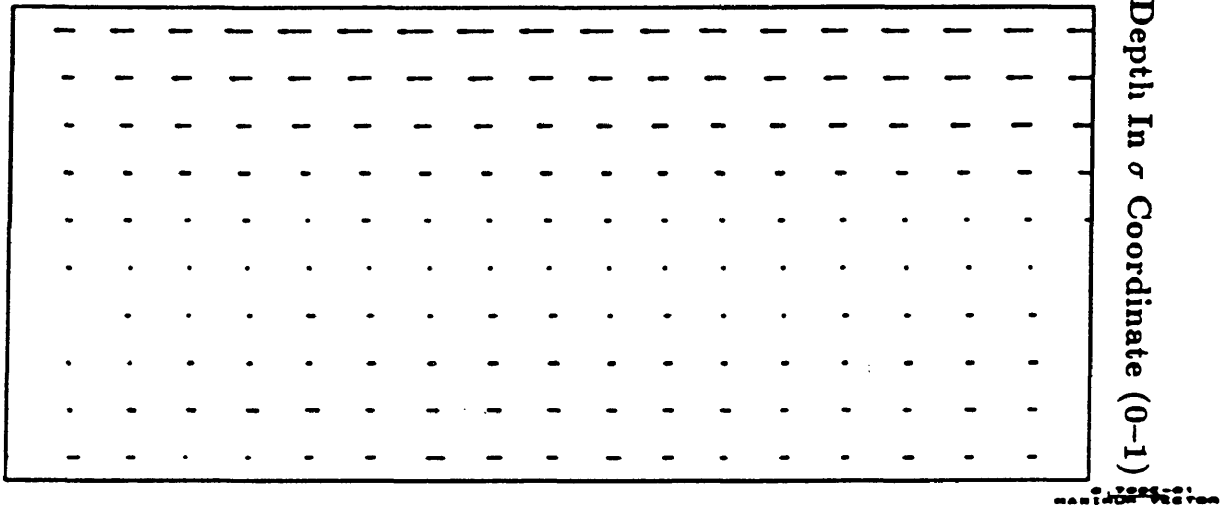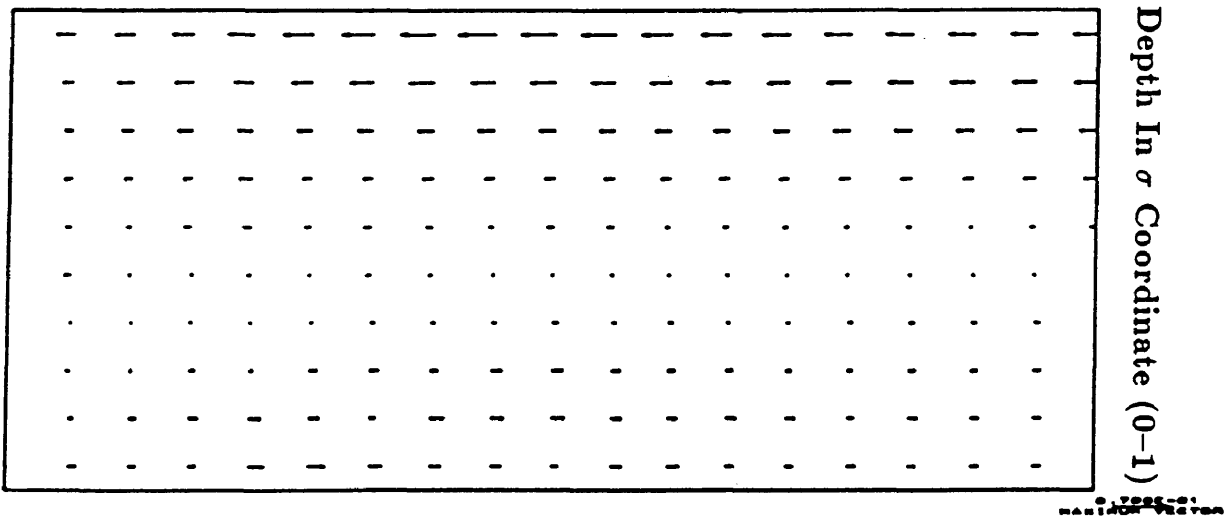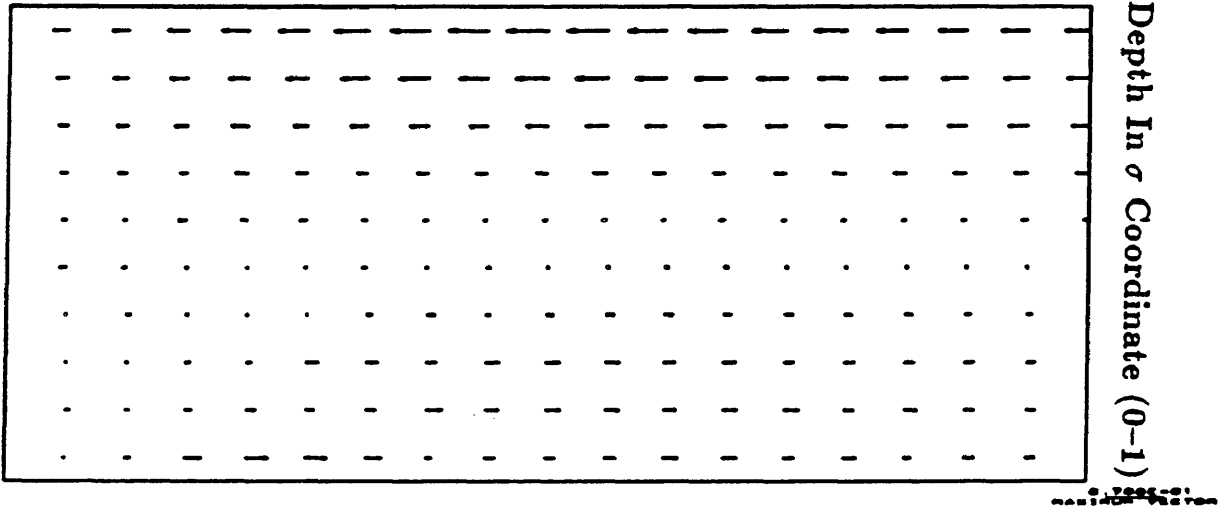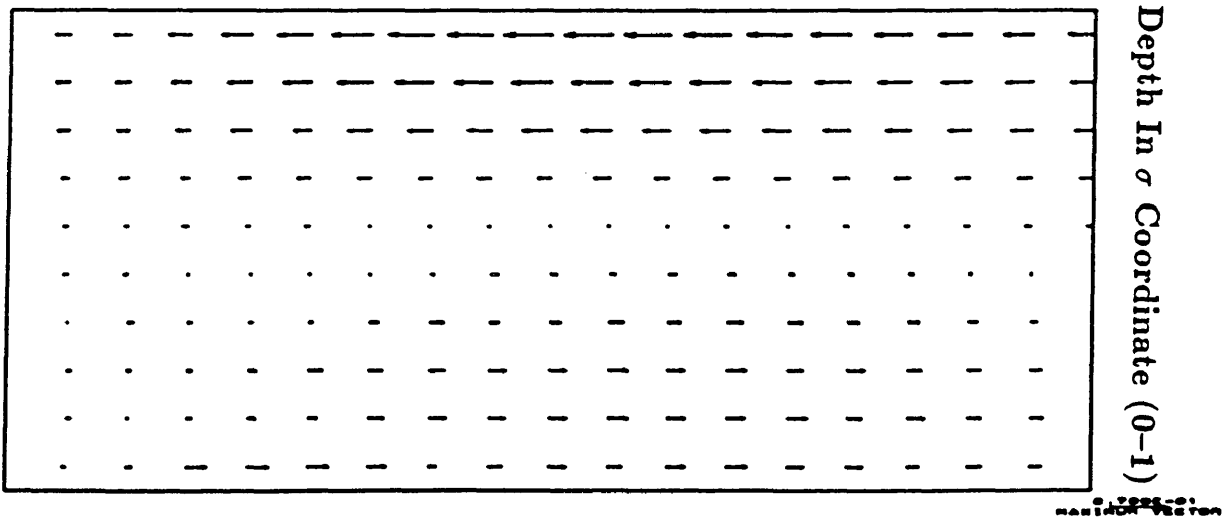

Channel Length 150 Km

10 Days After Spring Tide

Channel Length 150 Km

6.4.4   Residual Vector Potential Transport Velocity

The Lagrangian residual transport velocity equals the sum of the Eulerian residual transport velocity and the vector potential transport velocity, (Hamrick, 1990)

$$u_{lag} = u_{er} + u_{vec}$$

where

$$u_{er} = \langle u_1 \rangle + \frac{\langle h_0 u_0 \rangle}{h}$$

i.e.

$$u_{er} = \langle u_1 \rangle + \text{wave transport}$$

$$u_{vec} = -\frac{1}{h} (\partial_z B_y)$$

It is noted that the Eulerian residual transport velocity defined here is in a stretched vertical coordinate and satisfies the continuity equation, whereas vector potential transport velocity is one part of the Stokes drift. This relation is interesting since it shows the Lagrangian residual transport velocity can either be changed by variations in the Eulerian residual transport velocity, the vector potential transport velocity, or both.

To show the modulation of the vector potential transport velocity with the spring-neap tide forcing more clearly, two representative sections are selected. One is near the mouth of the channel, 30 km from the mouth, and the other is at the mid-channel, 75

89

km from the mouth. The vertical profiles of the vector potential transport velocity for these two sections at neap and two days before spring tide are presented in Figure 6.14 and Figure 6.15. The vertical scales are the same for the two sections to make it easier to compare the values of the vector potential transport velocities. It is important to note that the vector potential transport velocities at both sections oppose the Lagrangian transport velocity in the surface as well as in the bottom layers, though during neap tide their values are relatively small. For the section near the mouth (30 km), the vector potential transport velocity is greater in magnitude than the vector potential transport velocity at the mid-channel. The maximum values of the vector transport velocity near the mouth is about plus or minus 0.30 cm/sec during spring tide while at the mid-channel, the maximum value of the vector transport velocity is about plus or minus 0.12 cm/sec.

Figure 6.14   Vector Potential Transport Velocity at 30 Km from

the Channel Mouth
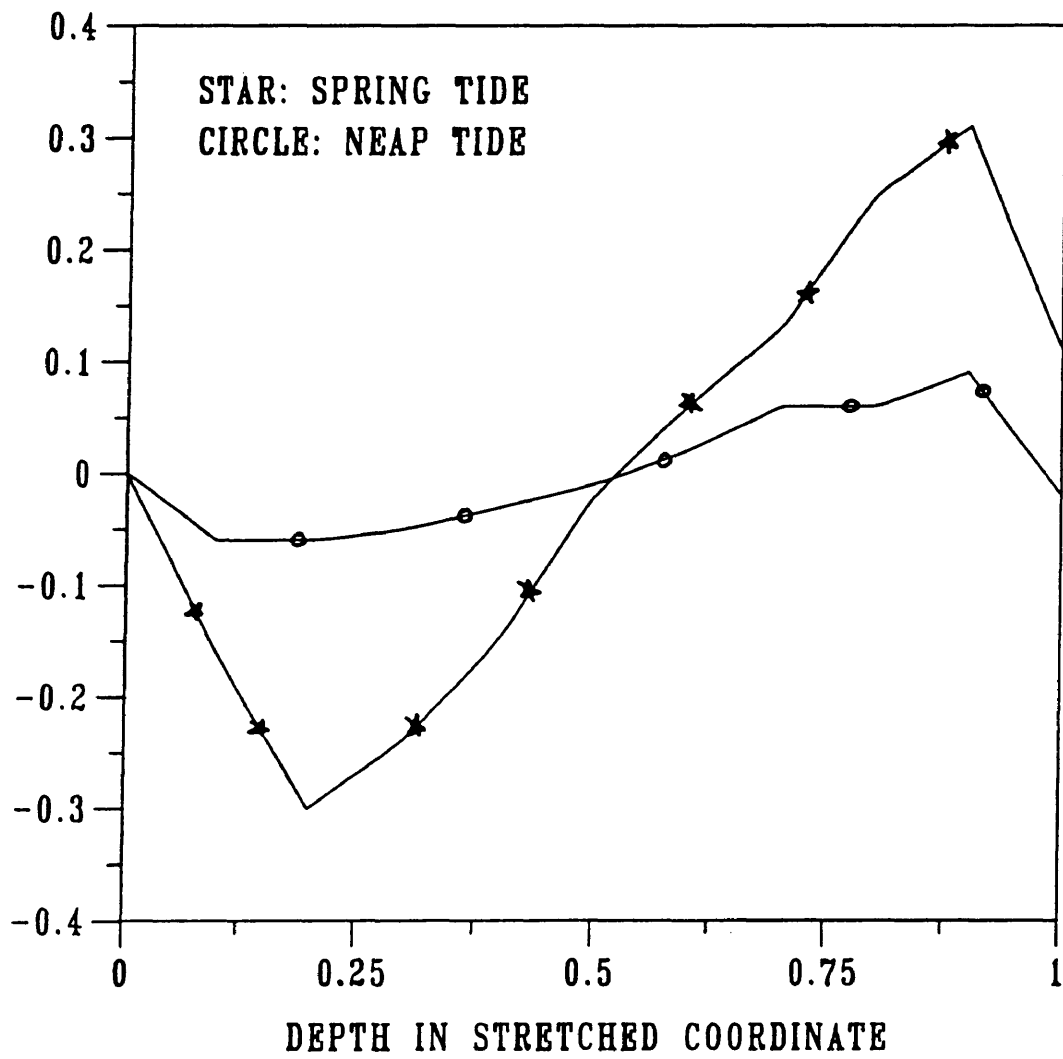
Figure 6.15   Vector Potential Transport Velocity at 75 km from

the Channel Mouth
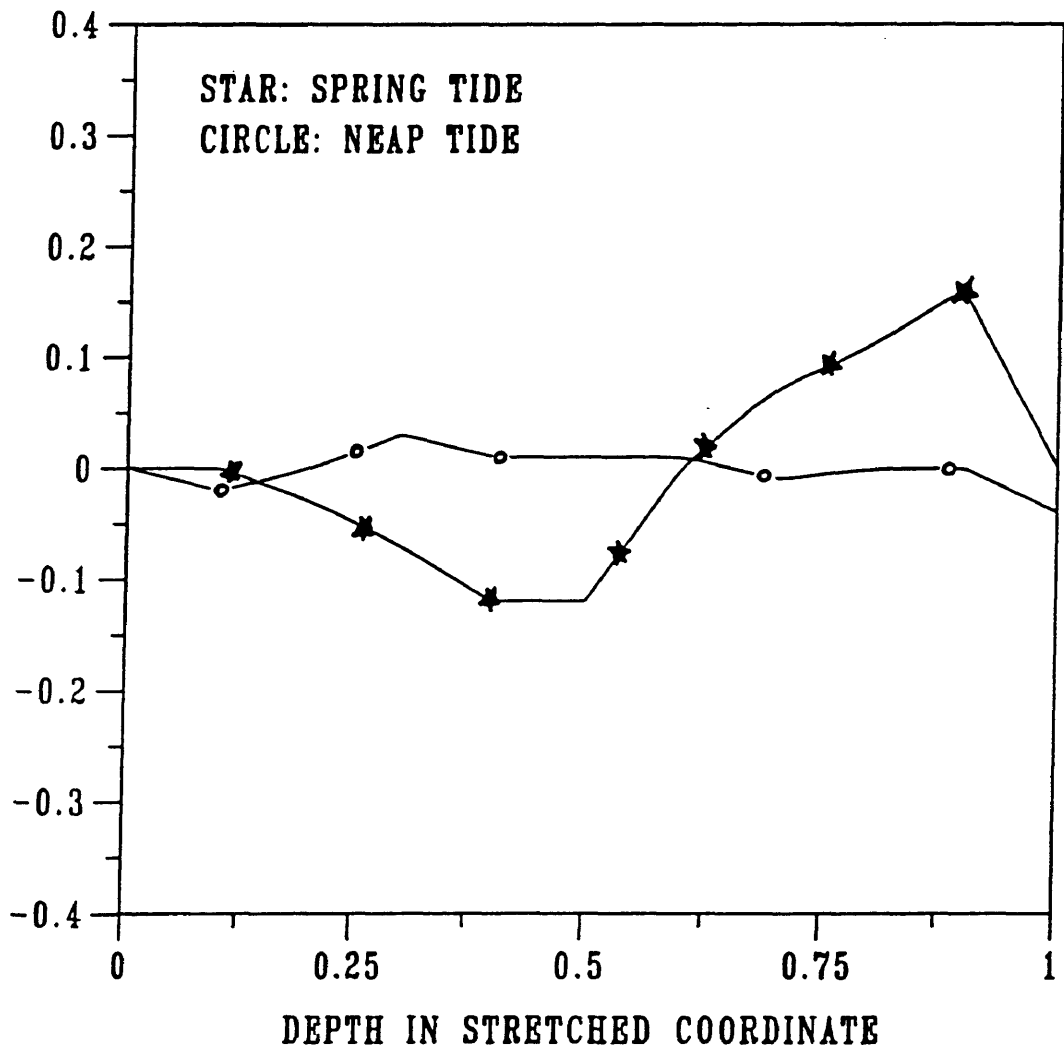
6.5   Discussion of Results

One objective of this numerical simulation was to investigate the relative importance of the modulation of the residual transport velocity in the process of the de-stratification of an estuary with a spring-neap tide forcing. In particular, the hypothesis that spring-neap modulation of the Stokes drift is a significant factor in the modulation of the Lagrangian residual circulation and stratification was posed for investigation. The results of the numerical experiment indicated that two different locations in the estuary channel need to be considered. One location is near the mouth of the channel and the other is at the mid-channel.

6.5.1   Circulation and Stratification Near the Channel Mouth

First consider the case which is close to the mouth of the hypothetical estuary, i.e. 30 km from the mouth. The Lagrangian residual transport velocity at neap and spring tide, as well as the vector potential transport velocity, a component of the Stokes drift, during spring tide were plotted against depth in Figure 6.16. The Lagrangian residual velocity is weaker during spring tide compared to its neap tide magnitude both in the surface and in the bottom layers. It is quite interesting that the magnitude of this decrease in the Lagrangian transport velocity can in large part be accounted for by the opposing vector potential transport velocity with Eulerian residual currents having little effect on the change in modulation of the Lagrangian residual transport. Looking back to Figure 6.2 to Figure 6.5, which give the modulated salinity distribution along the channel, it clearly shows that, at 30km from the mouth, the water

column is well mixed throughout the spring-neap tide forcing period. There is likely no change of the Eulerian residual current associated with the stratification and destratification of the water column or the turbulent mixing. It can be concluded that near the mouth where the water column is well mixed, the vector potential transport velocity plays a primary opposing role, weakening the Lagrangian residual velocity in both the surface and the bottom layers, while variations in the Eulerian residual currents are not significant. In this case, the vector potential transport velocity does not affect the stratification or de-stratification of the water column, since it is always well mixed during spring-neap tide forcing period.

Figure 6.16   Comparison of Vector Potential Transport Velocity

at Spring with Modulated Lagrangian Residual

Velocity at Spring and Neap at 30 km from the

Channel Mouth
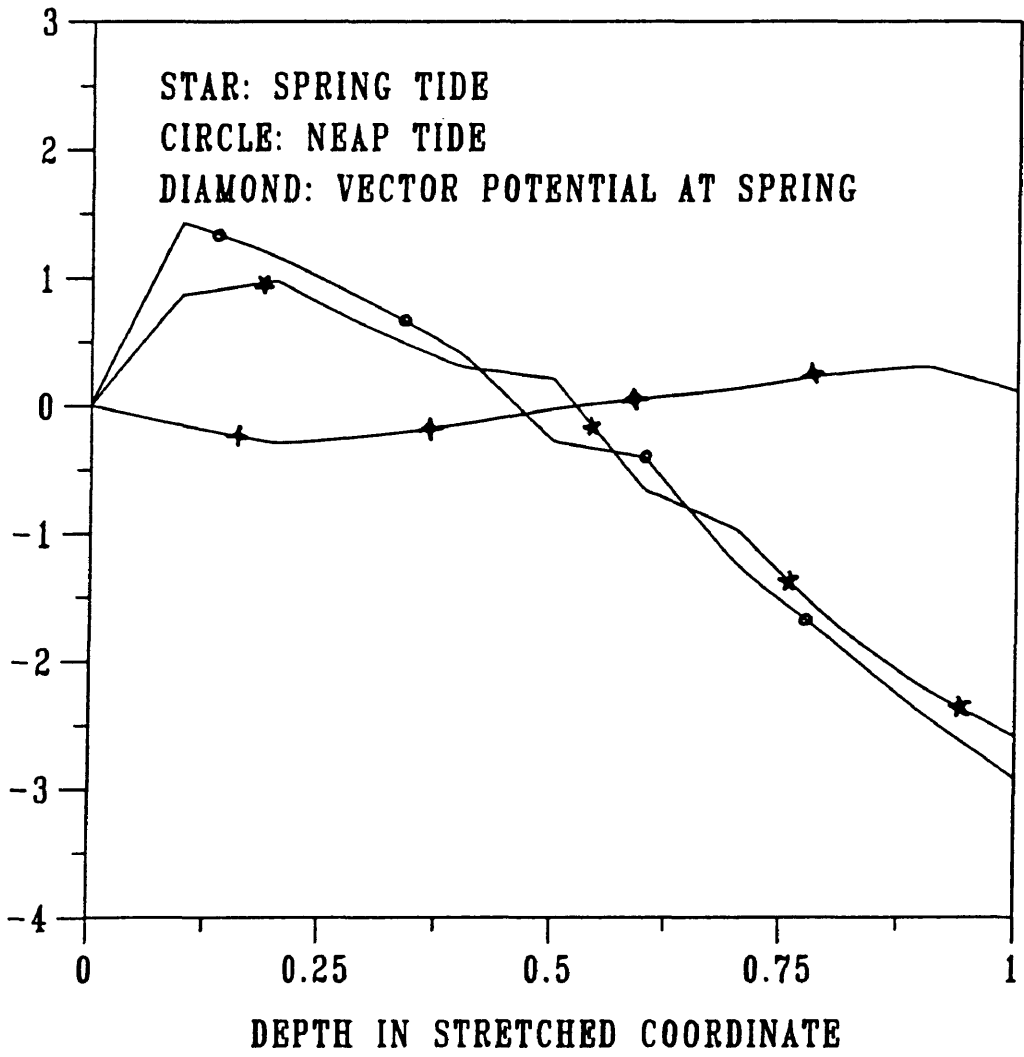
6.5.2   Circulation and Stratification Near the Channel Middle

The second case deals with the mid-channel region. Just as in the first case near the channel mouth, the Lagrangian residual transport velocity at both the neap and 2 days before the spring tide are plotted against the depth in Figure 6.17. The vector potential transport velocity is also plotted as a comparison to investigate its role in the destratification of the estuary. At mid-channel, the estuary shows clearly the process of the stratification and de-stratification cycle (Figure-6.2 to Figure-6.5) with the spring-neap tide forcing. From Figure 6.17, it is clear that the magnitude in Lagrangian residual transport velocity is reduced by about 1.6 cm/sec both at the surface and bottom of the water column during the spring tide period. The vector potential transport velocity during the spring tide period is very small compared to the changes in the Lagrangian residual current, though it is opposing the Lagrangian residual current. Since the Lagrangian residual velocity is equal to the sum of the Eulerian residual transport velocity and the vector potential transport velocity, if the vector potential transport velocity is too small to account for the modulation of the Lagrangian residual transport, it is clear that the decrease in the Lagrangian residual current is mainly because of the decrease of the Eulerian residual current which mainly consists of the density driven residual current.

Figure 6.17   Comparison of Vector Potential Transport Velocity

at Spring with Modulated Lagrangian Residual
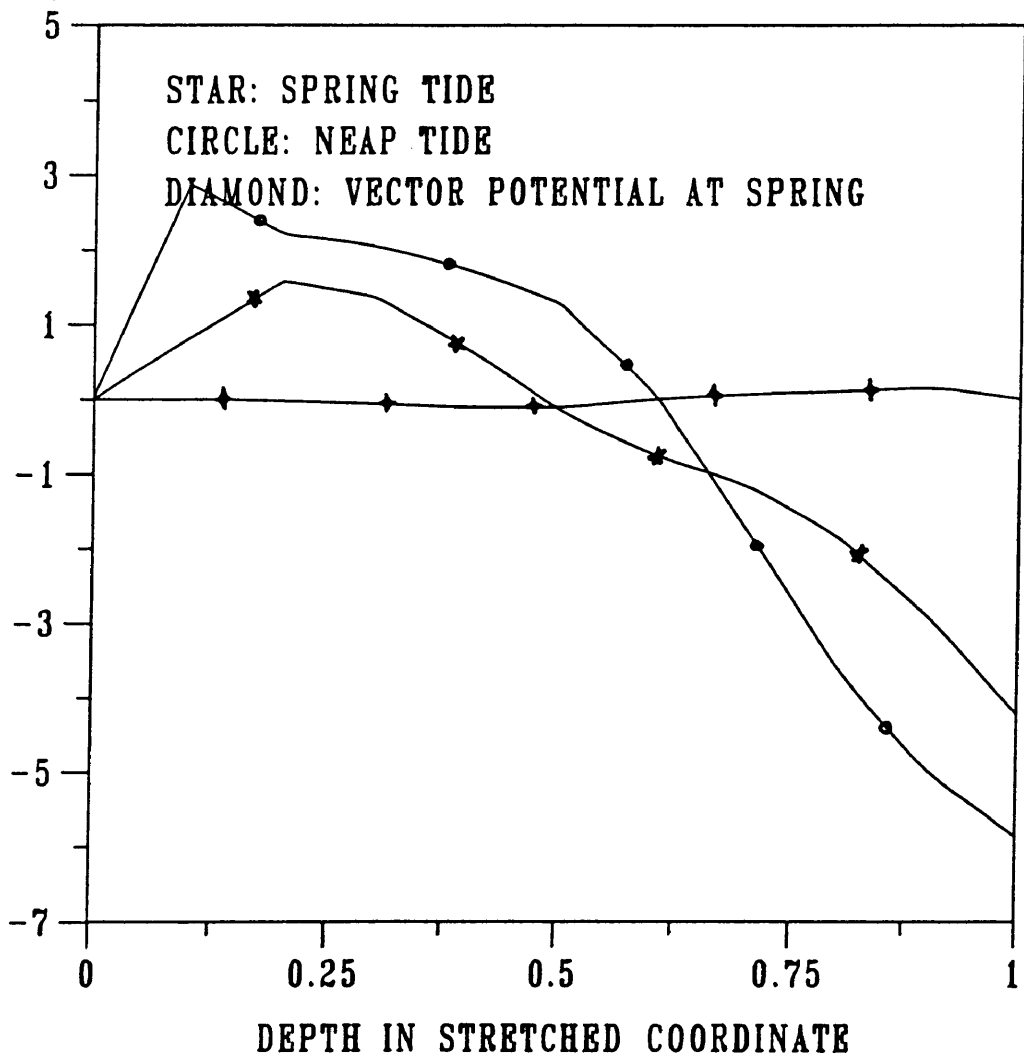
Velocity at Spring and Neap at 75 km from the

Channel Middle

STAR: SPRING TIDE
CIRCLE: NEAP TIDE
DIAMOND: VECTOR POTENTIAL AT SPRING

VELOCITY IN CM PER SEC

DEPTH IN STRETCHED COORDINATE

According to the analysis of Ianniello (1977), the relative magnitudes of non-linearly induced currents and density induced currents can be estimated as follows:

$$\frac{u_D}{u_N} = \frac{h_0^2 \, \overline{(\Delta\rho)}_x}{\eta_0^2 \, \rho_0}$$

where u_D is the density induced residual current and u_N is the non-linearly induced current. With the parameters used in the numerical experiment, for spring tide, h_0 = 10 meter, η_0 = 0.54 meter, $\overline{(\Delta\rho)}_x / \rho_0$ = 0.015, ρ_0 = 1.0 gram per cubic centimeter, the ratio between the density induced residual and the non-linear interaction induced residual current u_D/u_N is about 6. Thus the density driven current is about 6 times the non-linearly induced currents.

The decrease in the Lagrangian residual current in the mid-channel is mainly due to the weakening of the Eulerian residual current which mainly consists of the density induced residual current. The weakening of the density induced residual current results directly from the de-stratification of the water column in the mid-channel, as a result of the stronger turbulent mixing during the spring tide period. It is concluded that at the mid-channel, the de-stratification of the water column mainly results from a stronger turbulent mixing because of the stronger spring tide forcing, whereas the non-linearly induced Eulerian residual current, like the vector potential residual

current which is a component of the Stokes drift, is only of secondary
importance in the process of the de-stratification of the middle
region of the estuary.

7. Summary

A two dimensional (vertical plane) estuary model with an algebraic stress/flux turbulence model (level-2) was developed to simulate a real time 2-D vertical flow in a hypothetical estuary with a length of 150 km and a depth of 10 meter. The main advantage of the turbulence model used here is that there is no need to tune the empirical turbulence model parameters for different estuaries, since all the empirical parameters are determined by the laboratory experiments in the neutral turbulent flow. It also reflects the estuarine physical mixing process more realistically since the eddy viscosity and diffusivity are time-dependent and can change instantaneously (more precisely, change values every 18 minutes) according to the physics given by the turbulence model without the artificial constraints (Elliot, 1976, Wang, 1980). Based on the experience gained by the use of the algebraic stress/flux turbulence model in the 2-D vertical model, it is suggested that this turbulence model be extended to three-dimensional models in the future.

A numerical experiment was conducted using the model. The residual salinity, eddy diffusivity, Lagrangian current, Eulerian current, and vector potential transport current were all filtered out from the instantaneous output of the numerical simulation with a spring-neap tide forcing by a least squares filter built into the

program. The modulated salinity distribution along the channel shows characteristics of a typical partially mixed estuary. In the mid-channel region where the horizontal salinity gradient is strongest, the stratification and destratification of the water column are clearly shown to be modulated by the spring-neap tide forcing. The vertical profiles of eddy diffusivity at the mid-channel show a typical valley with two maximums during neap tide period and are modulated by the spring-neap tide forcing. During the period of the spring tide, the valley of the eddy diffusivity profile disappears because of stronger vertical mixing. The Lagrangian residual currents show a characteristic two-layer circulation pattern and the strength of the two layer circulation is also modulated by the spring-neap tide forcing at the mid-channel. The modulated vector potential transport velocity opposes the Lagrangian residual velocity both in the surface and the bottom layers, and is larger near the mouth and smaller at the mid-channel. Near the mouth, the water column is mixed vertically, and the modulation amplitude of the Lagrangian residual currents is relatively small. The vector potential transport is mainly responsible to the reduction of the Lagrangian residual velocity during spring tide period. Since the vector potential transport velocity has a relatively large value near the mouth of the channel compared to its values at the mid-channel, this result should be observed by field measurements near the mouth of the estuary.

At the mid-channel, the change of the Lagrangian residual velocity during the spring-neap tide forcing is relatively larger than the changes in the vector potential transport velocity. The opposing

vector potential transport velocity can not account for the changes in the Lagrangian velocity resulting from the spring-neap tide forcing. Since the Lagrangian residual is equal to the sum of the Eulerian residual and the vector potential transport velocity, the weakening of the Lagrangian residual currents during the period of spring tide can be explained as a result of the weakening of the Eulerian residual currents which is mainly caused by the stronger vertical turbulent mixing. It is therefore concluded that at the mid-channel region where the stratification and destratification cycle is prominent with spring-neap tide forcing, the vertical turbulent mixing is mainly responsible for the destratification of the water column while the vector potential transport velocity component of the Stokes drift, plays only a secondary role.

Throughout the hypothetical estuary, the Lagrangian residual currents are weakened during the period of spring tide. This result is very interesting since, intuitively, during spring tide period, the tracer should be transported more rapidly because of stronger tidal currents. Since it is generally accepted that the long term transport of the tracer in an estuary is mainly a convective process which is determined by the Lagrangian residual circulation (Feng et al., 1986), the results of this study show that the rate of long-term transport of the tracer is reduced during spring tide because of the weakening of the Lagrangian residual currents which result from the increased opposing vector transport currents (near the mouth) and the increased vertical turbulent mixing (at the mid-channel). This point should be further explored in the future by field measurements.

Literature Cited

Arakawa, A. Design of the UCLA general circulation model. Numerical

   Simulation of Weather and Climate, Dept. of Meteorology, Univ.

   of California, Los Angels, Tech. Rept. 7, 116 pp. 1972.

ASCE Task Committee on Turbulence Models in Hydraulic Computations.

   Turbulence modeling of surface water flow and transport. J. of

   Hydraulic Engineering. Vol. 144, No. 9, pp 970-1014, 1988

Bowden, K. F. Circulation and diffusion in Estuaries. G. H. Lauff

   (ed). American Association for the Advancement of Science,

   Washington, D. C. 757pp. 1967.

Cheng, R. T., Euler-Lagrangian computations in estuarine

   hydrodynamics, in Proceedings of Third International

   Conference on Numerical Methods in Laminar and Turbulent Flow,

   edited by C. Taylor, J. A. Johnson, and R. Smith, Pineridge

   Press, Swansea, United Kingdom, pp. 341-352, 1983

Elliot, A, J. A numerical model of estuarine circulation in a

   branching tidal estuary. Chesapeake Bay Institute, Rep. 54,

   The John Hopkins University, Baltimore, MD. 85 pp. 1976.

Feng S. Z., Cheng, T. R., Xi, P. G. On tide induced Lagrangian
residual current and residual transport. I: Lagrangian
Residual Current, II: Residual Current With Application in
South San Francisco Bay. Water Resourcees Res., Vol. 22
No. 12, pp. 1623-1646, 1986.

Hamrick, J. M. The dynamics of long-term mass transport in estuaries.
in Residual Circulation and Long Term Transport in Estuaries
and Bay, Spring-Verlag. R. T. Cheng, ed. 1990

Hansen, D. V. Rattray, M. R. Gravitational circulation in straits and
estuaries. J. of Marine Res., 23, pp. 104-122, 1965.

Hansen, D. V. Salt balance and circulation in partially mixed
estuaries. in Estuaries. G. H. Lauff (ed). Publication No. 83,
American Association for the Advancement of Science,
Washington, D. C. 757 pp. 1967.

Hudson, Robert Y. et al. Coastal Hydraulic Models. Special Report No.
5, US Army Coastal Engineering Research Center, Fort Belvoir,
VA 1979.

Kolmogoroff, A. N. The equations of turbulent motion in an
incompressible fluid. Izv. Akad. Nauk SSSR, Ser. Fiz., 6,
No. 1, 2, pp. 56-58, 1942.

Ianniello, J. P. Tidally induced residual currents in estuaries of
constant breadth and depth. J. of Marine Res., 35(4),
pp. 755-786, 1977.

Krauss, W. Dynamics of the homogeneous and quasi-homogeneous ocean.
Gebruder Borntraeger, Berlin, 300pp. 1973.

Longuet-Higgins, M. S. On the transport of mass by time-varying ocean currents. Deep-Sea Res., 16:431-447, 1969.

Mellor, G. L. Yamada T. A hierarch of turbulence closure models for planetary boundary layers. J. Atmos. Sci., 31, 1791-1806, 1974.

Mellor, G. L. Yamada T. Development of a turbulence closure model for geophysical fluid problems. Rev. Geoph. Sp. Phy., 20, pp. 851-875, 1982.

Mesinger, F. Arakawa, A. Numerical methods used in atmospheric models. W.M.O. Tech. Note, pp. 17-64, 1976.

Oey L. Y., Mellor G. A three dimensional simulation of the Hudson-Raritan estuary. Part I, II, III. J. of Phys. Ocean. Vol. 15, pp. 1676-1720, 1985.

Prichard, D. W. A study of the salt balance in a coastal plain estuary. J. of Marine Res., 13(1), pp. 133-144, 1954.

Prichard, D. W. The dynamic structure of a coastal plain estuary. J. of Marine Res., 15(1), pp. 33-42, 1956.

Rodi, W. Mathematical modeling of turbulence in estuaries Sonderforschungsbereich 80, Univ. of Karlsruhe, Karlsruhe, FRG, 1978.

Rotta, J. C. Statistische theorie nichthomogener turbulenz. Z. Phys., 129, pp. 547-572, 131, pp. 51-77, 1951.

Ruzecki, E. P., Evans, D. A. Temporal and spatial sequencing of

  destratification in a coastal plain estuary. Lecture Notes on

  Coastal and Estuarine Studies, 17, pp. 368-389, 1986.

Simons, T. J. Circulation models of lakes and inland seas. Canadian

  Bulletin of Fisheries and Aquatic Sciences, Bulletin 203,

  1980.

Wang, D. P., Kravitz, D. W. A semi-implicit, two-dimensional model

  of estuary circulation. J. of Phys. Ocean., Vol. 10,

  pp. 441-454, 1980.

Westerink, et al. A frequency domain Finite Element Model for tidal

  circulation. Energy Laboratory, pp. 79-97, MIT. 1985.

Yamada, T. The critical richardson number and the ratio of eddy

  transport coefficients obtained from a turbulence closure

  model. J. Atmos. Sci., 32, pp. 926-933, 1975.

VITA

SAN JIN

Born in Shanghai, China, 28 February 1950. Earned B.S. in Physics from Fu Dan University in 1982. Taught for three years in Shanghai Fishery's University. in Shanghai, China. One year graduate study in Biomedical Engineering in Shanghai Jiao Tong University. Entered master program in College of William and Mary, School of Marine Science in 1986.